# Alternative concept on space used in the BSM – Supergravitational Unified Theory unveils the connection between the micro-cosmos and Universe

**Stoyan Sarg Sargoytchev, PhD**
**World Institute for Scientific Exploration**
http://instituteforscientificexploration.org/ise-directors-advisors/

**Abstract:** The theory is based on an original alternative space-time concept that leads to a new vision of the micro-cosmos and Universe. The relationship between the forces in Nature is unveiled by adopting the following framework: (1) Empty space without any physical properties and restrictions; (2) Two fundamental particles of superdense protomatter with parameters associated with Planck's scale; (3) A Fundamental law of Supergravitation (SG) with forces inversely proportional to the cube of distance in a pure empty space. An enormous abundance of these two particles, with vibrational energy beyond some critical level, can congregate into self-organized hierarchical levels of 3D formations, governed by the SG law. The process leads deterministically to the creation of space with quantum mechanical properties and a galaxy as an observable mattter. The fundamental SG law is behind the gravitational, electric, and magnetic fields and governs all kinds of interactions between the elementary particles in the space of the physical vacuum. Analysis of cosmological observations reveals that the galaxies possess their own cycle in which the elementary particles are formed at a hidden non-observable phase. The problem of departure of the Hubble plot from the predicted one is solved, showing that the redshift is not of Doppler origin. The conclusion is that the Universe is stationary and eternal.

**Keywords: physical vacuum, space-time, unified theory, quantum gravitation, zero point energy, cosmological redshift.**

## Introduction.

Contemporary theoretical Physics is plagued with problems in several fields: Particles Physics, Quantum Mechanics, Theory of Relativity, and Cosmology. Most of the physical models in different fields are mainly mathematical constructs that does not describe exactly the physical reality. When trying to connect them, they are contradictable, so they may not provide the real picture of the microcosmos and Universe. The Big Bang model also has numerous problems, indicating that the galactic redshift might not be of Doppler type. One of the proofs is the distribution of the quasars showing that they are not at the "edge" of the observable Universe [1]. The main reason for all these problems is the concept of space, known as a physical vacuum, adopted 100 years ago. James Clerk Maxwell, the father of Modern Physics developed Classical Electrodynamics with the assumption of material Ether. This is evident from his famous work "A Treatise on Electricity and Magnetism, section "A medium is necessary", p. 493 [2]. After the inconclusive Michelson-Morley experiment, Einstein formulated in 1905 his postulate of Relativity, opposing the idea of the Ether, but after he developed General Relativity in 1920, he reversed partly his opinion claiming that the Ether is necessary [3]. At the same time, he still envisioned the Ether as a non-material substance, which diverted the search from the direction envisioned by Faraday, Maxwell, Lord Kelvin, and many other famous scientists. The only argument of Einstein against the material Ether presented in his book "Sidelights of Relativity" [3] is that "neither Maxwell nor his followers succeeded in elaborating a mechanical model for the ether". Einstein, however, did not present any proof that the concept of material Ether is impossible. Presently, after the proof that different types of laboratory experiments detect our absolute motion through some real substance [4-13], it was understood that the Michelson-Morley experiment had a methodological error. Additionally, the Casimir's forces have been discovered 35 years later than Einstein's statement, but nobody so far guessed that they might be a signature of the most fundamental law in Nature – a Law of Supergravitation.

## New approach

The new approach began with a search of a possible physical model of the underlying substance of space, known as Aether and its physical relation with the elementary particles. The guess and formulation of one most fundamental physical law called a Supergravitational low was the useful starting point. This law permitted unveiling the superfine substance of space, known as the physical vacuum to go beyond Newton's laws of gravity and inertia and Einstein's theory of Relativity. While the search for a correct physical model of this substance has been officially abandoned, it was the most useful starting point in the development of the "**Basic Structures of Matter – Supergravitation Unified Theory**" (BSM-SG) [14-25].

## Analysis and results

Extensive analysis of experimental data from different fields of physics and accumulated astronomical observations led to the development of a unified theory with the following framework:

- **Two superdense indestructible fundamental particles (FPs) with a spherical shape of two different substances of protomatter** with a radius ratio of 2:3 and different densities. The bell-shape curve radial dependence of their density permits a central of mass type of vibrations of the FP individually and in 3D formations. They are able to vibrate at extremely high proper frequency, the average (for both types FPs) value of which is associated with the Planck's frequency given by the expression:

$$F_{PL} = [(2\pi c^5)/(Gh)]^{1/2} = 1.855 \times 10^{43} \ (Hz)$$

- A fundamental **law of Super Gravitation (SG),** governs the interactions between FPs in a **classical void space**, according to which FPs from the same substance interact by a force inverse proportional to the cube of the distance. The SG law in empty space is given by Eq. 1.

$$F_{SG} = G_O \frac{m_{01}m_{02}}{r^3} \qquad (1)$$

where: $F_{SG}$ is the SG force, $m_{01}$, $m_{02}$ - intrinsic protomatter mass, r – distance; $G_O$ - is a SG constant, which is different for both protomatter substances and may change the sign for a case of imbalanced geometrical formations

- **Vibrational energy and SG law:** FPs preserve a limited freedom of vibrations in geometrical formations from the same type of substance. In a complex 3D structure, FPs may vibrate within a saturation limit – an energy well of the structure. SG law could be associated with the necessary energy for filling the energy well. The SG attraction between FP formations of different substances in a uniform lattice (discussed later) may not be so strong or could even convert to repulsion at different mutual distance due to the different time constants of both FPs.

The suggested physical model allows using a classical approach in a real 3-dimensional space with unidirectional time, so the principles of causality, objectivity, and logical understanding are completely preserved. The derived physical models exhibit excellent properties when they are applied for analysis of numerous experiments and observations from the range of particle physics to cosmology. This is demonstrated in BSM-SG theory. Based on that analysis, a cosmological scenario is presented in Chapter 12, which can be briefly summarized as follows:

**The enormous abundance of these two Fundamental Particles with energy above some critical level is driven by the SG law into the self-organized hierarchical level of 3D formations. This is a unique process of crystallization leading deterministically to the creation of the elements of space with quantum properties – physical vacuum and the elementary particles forming the observable matter in the Universe. This process is possible in a volume of enormous concentrations of the FPs which corresponds to the so-called "black holes" detected at the centers of each well-formed galaxies. However, it takes place in a particular invisible phase of each galaxy.**

Under SG law, the matter is organized in hierarchical levels of 3D formations based on 3D geometry. Fig. 1, shows consecutive types of 3D formations at the lowest level of hierarchical order. They are denoted as Primary Tetrahedron (TH), Quasipentagon (QP) and Quasiball (QB).
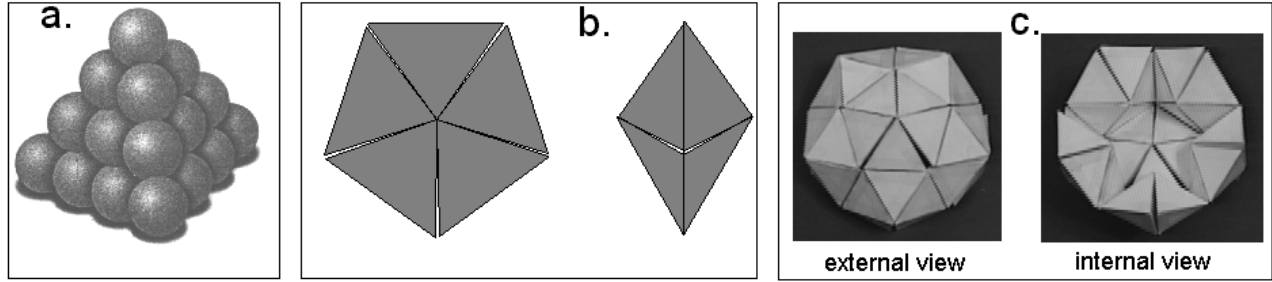
Fig. 1. Structures of lowest level. a. Tetrahedron (TH), b – Quasipentagon, c. – Quasiball (QB)

The next stage contains the same type of formations, while the TH is formed by QBs of previous stage. The rotational internal SG modes are strongest at TH with SG field stronger at the edges. This keeps the formations and constant number between formations of same type and order. The SG modes in QP exhibit an axial anisotropy due to its geometrical shape. The gaps between the THs in QP are combined in a common gap of $7.355^0$, which is preserved in QB. This allows a left or right-hand twisting of the QB - this is a **lowest level memory carrying the chirality (handedness)**. The sectional view of QB shows that this formation encloses an internal empty space.

1 QB = 12 QP = 60 PT – equation of constant intrinsic matter quantity (valid for any upper-order formations of the same type)

The BSM-SG theory helped to unveil the physical origin of the dimensionless fine structure constant, $\alpha$, one of the mysterious constants that bothered the mind of physicist for decades [10]. It appears that it is a signature of a specific vibrational mode of the Primary Tetrahedron. Its reciprocal value $1/\alpha = 137.035999$, where the integer 137 = n – is the number of sub-cycle in one full cycle and 0.035999 is the sub-cycle as a fraction of the full cycle. The derived theoretical formula is given by the expression (2).

$$\alpha_{th} = 2/[(n^2 + 2\pi^2)^{1/2} + n] = 7.29735194 \times 10^{-3} \text{ - Sarg's formula} \qquad (2)$$
$$\alpha = 7.297352533 \times 10^{-3} \qquad \text{(CODATA 98)}$$

The Sarg's formula value differs from the experimental value adopted by CODATA 98 by 0.000008% only. The conclusion is that it is a natural irrational number like pi. While pi, however is defined in a 2D space, the fine structure constant is related to a vibration property of the specific formation of the Primary tetrahedron in 3D space.

Fig. 2. illustrates the hypothetical consecutive phases of the primordial matter evolution from both FPs leading to the crystallization of elementary particles. This process takes place in a hidden phase of the evolution of every individual galaxy before it is born by explosion, whose detectable signature is a super-strong Gamma Ray Burst. This is a cosmological event in which a new galaxy is born in the void space occupied by the previously collapsed one. The free prisms form a Cosmic Lattice (CL) in the empty, while the stable elementary particles - protons, neutrons, and electrons firstly form simple atoms, such as hydrogen, deuterium, tritium, helium. The newborn CL space has all known properties of the physical vacuum and may have a higher Zero Point Energy, which will be detected as a blue galactic redshift (for example, Andromeda galaxy).
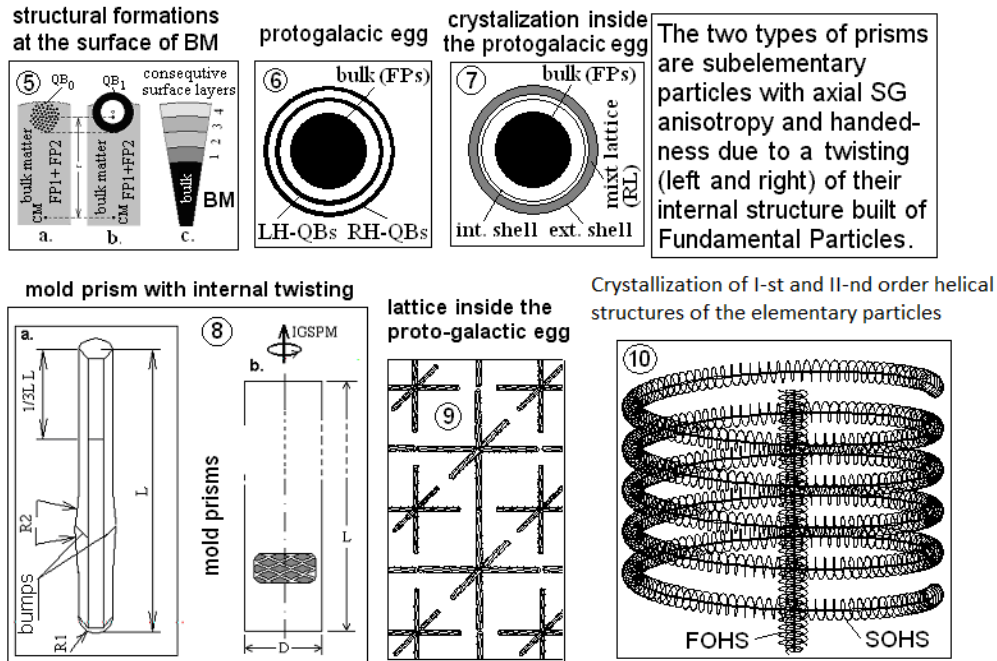
Fig. 2. Phases and structural 3D formations at lower level of matter organization leading to creation of the particles called prisms, from which the superfine structure of the space and elementary particles are built.

The properties of the CL space are the following:
- The CL space is formed of alternatively arranged CL nodes made of 4 prisms of the same type, which have intrinsically small inertia in a void space
- The distance between the CL nodes is kept by the SG forces the sign and strength of which depend on the distance due to the different time constants of the two FPs .
- CL space possesses quantum and space-time properties and Zero Point Energy, which includes two components: a Static (strong one) and a Dynamic (weak one)
- The SG field between the elementary particles in CL space is propagated by the ***abcd*** set of axes (see Fig. 3) of the CL nodes and appears as a Newtonian gravitation
- The Electrical and Magnetic fields are types of CL space modulation, based on the dynamic properties of the CL nodes involving mostly momentums along the ***xyz*** set of axes.
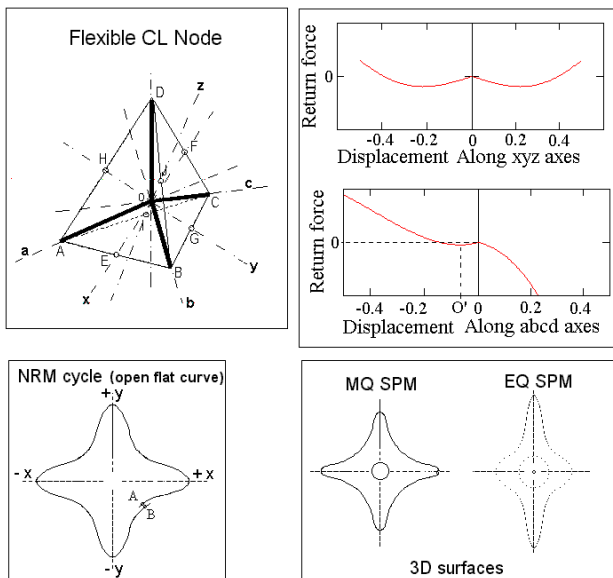


Fig. 3 illustrates the 3D geometry of CL node, and its dynamic vibrations. The CL node is formed by 4 prisms of the same type of FP's held by SG forces. Its dynamics under SG law is described by two vectors: Node resonance momentum (NRM) and Spatial Precession Momentum (SPM). The hodograph of NRM (cycle) is an open flat curve, as shown in Fig. 3. However, a large number of NRM cycles forms a closed surface called Quasisphere with 6 bumps (along xyz axes) and 4 depressions (along abcd axes). MQ is a magnetic Quasisphere of SRM vector (with central symmetry), while EQ is an Electrical Quasisphere of SPM vector involved in Electrical lines. MQs (or EQs) involved in magnetic (or electrical lines) are phase synchronized, but their SPM frequencies are different. The energy of EQ is larger than MQ. The photon is a wave with a helical configuration involving EQs and

Fig. 3.

4

the boundary of MQs. The MQs at the boundary assure the preservation of the quantum energy of the photon during its propagation. During this propagation the energy momentum from every CL node included in the wavetrain transfers to a neighboring one for one NRM cycle – this defines the velocity of light. The transfer through a large number of CL nodes is in a helical path with a step defining the photon wavelength. The rotation of electrical and magnetic vectors are caused by the asymmetry of the CL node axes (*xyz*, and *abcd*). The velocity of light is additionally strongly stabilized by the effect of self-synchronization between the CL nodes, which is with the SPM (Compton's) frequency and defines the permeability and permittivity of the physical vacuum (Chapter 2 of BSM-SG).

The **Elementary particles** are built of sub-particles denoted as prisms arranged in **helical structures** in a crystallization process preceding the birth of the galaxy.

Fig. 4 shows the overall shape and dimensions, of the electron, and the structure of its internal lattice (impenetrable for CL nodes.) The Electron is a one coil of <u>First Order Helical Structure</u> (FOHS) - an oscillating 3-body system with two proper frequencies [21]. The first one is the Compton frequency equal to the SPM frequency of the CL node. and its modulation on the CL nodes, appears as an electrical charge.
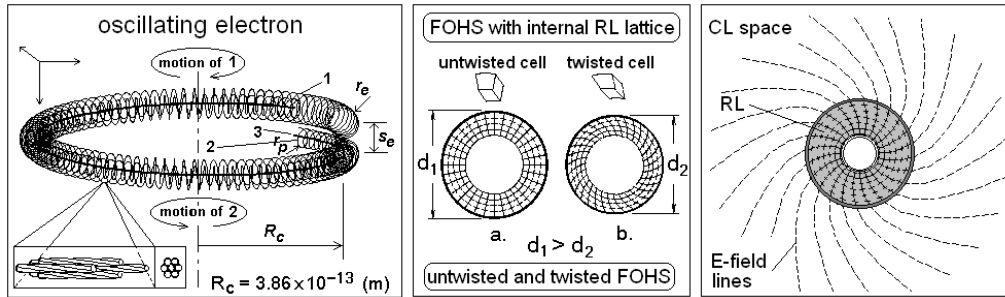


Fig. 4. Electron with its internal lattice modulating the CL space. Calculated dimensions: (m):

$$R_C = 3.86 \times 10^{-13}; r_e = 8.8428 \times 10^{-15}; r_p = \frac{2}{3} r_e$$

The fine structure constant is embedded in the helical step of the electron that is behind its anomalous magnetic moment.

$$s_e = (\alpha c / v_c)(1 - \alpha^2)^{1/2} = 2r_e = 1.7706 \times 10^{-14} \quad (m) \tag{3}$$

The derived euation for the anomalous magnetic moment of the electron is given by Eq. (3.a) (section 3.10 Chapter 3 of BSM-SG.

$$\mu_e = \frac{qh}{4\pi m_e}(1 + \frac{\alpha}{2\pi}) \quad [Am^2] \tag{3.a}$$

The **denser internal lattice of FOHS** modulates the CL space, creating aligned EQ SPM – **electrical field lines.** When moving and rotating, they cause formations of loops of phase synchronized MQs – **magnetic lines**.

**Confined motion:** The screw-like motion of the rotating and oscillating electron and its interaction with the SPM frequency of the CL nodes causes a confined motion with preferred velocities, corresponding to (13.6/n) eV, where **n** matches the principal quantum number of the Bohr atomic model. In a closed loop motion, **n** defines the real length of the quantum orbit [21], because the loop length contains a whole number of quantum magnetic lines - Comton's wavelength (See §7.7.1, Chapter 7 of BSM-SG).

## Cosmic Lattice parameters and mass equation

Using the unveiled structure and oscillating properties of the electron, the following physical parameters of the CL space are derived:

**Static CL pressure, P_S**:

$$P_S = \frac{m_e}{V_e} = \frac{g_e^2 h v_c^4 (1 - \alpha^2)}{\pi \alpha^2 c^3} = 1.3735 \times 10^{26} \quad (N/m^2) \tag{4}$$

**Partial CL pressure, P_P**: related to the inertial properties of the elementary particles in CL space at their confined motion

5

$$P_P = P_S \alpha \upsilon / c \quad (N/m^2) \quad \text{where: } \upsilon \text{ - is velocity} \tag{5}$$

**Dynamical CL pressure, $P_D$**: - exercised on atoms and molecules by ZPE waves responsible for equalization the CL space background energy.

$$P_D = \frac{h v_C}{c S_e} = \frac{g_e h v_c^3 (1-\alpha^2)}{2\pi \alpha c^3} = 2.0258 \times 10^3 \quad (\frac{N}{m^2 Hz}) \tag{6}$$

## Mass equation

**Static CL pressure divided on square of light velocity defines the Newtonian mass of elementary particle as a pressure exercised on its impenetrable volume of its FOHS (first order helical structure)**

$$m = (P_S/c^2)V_e \ (kg) \quad \underline{\text{mass (Newtonian) equation of the electron}} \tag{7}$$

where: $V_e$ – volume of impenetrable internal lattice of the electron

Using the dimensions of the electron shown in Fig. 3, the volume Ve on which the Ps exercises a pressure is

$$V_e = 2\pi^2 r_e^2 R_C = 5.96 \times 10^{-40} \quad (m^3) \tag{7.a}$$

For other stable particles proton neutron and positron the volume of their FOHS are proportional to their masses, so they can be obtained by the proportion to the mass of the electron – all they are known parameter.

**Then the mass equation for other particles is**

$$m = (P_S/c^2)V_e K_V \ (kg);$$

For proton: $K_V = m_p/m_e$ where mp and me are the masses of the proton and electron respectively

The formulation of the mass equation permits to unveal the mass deficiency in the nuclear reaction. The superdense protomatter in the elementary particles and especially protons and neutrons slightly shrinks the surrounding CL space in the near field. This is a microscopic effect of field curvature that slitly affects the parameter $P_S$ in the near field. In heavier atoms the shrunkage is greater. When number of protons or neutrons in the atomic nucleus changes in a nuclear reaction a mass deficiency occurs that is estimated by the Eisten equation $E = mc^2$. This is presented in the authors' books:

The signature of $P_D$ is unveiled in the observed Cosmic Microwave Background (CMB). Ne new spacetime concept leads to the conclusion that the observed CMB is not a relict radiation. The estimated background temperature of 2.72 K from the CMB is a signature of the wave fluctuations in the Cosmic Lattice that are also envisioned as a ZERO point energy The derived theoretical expression of this temperature in Chapter 5 of BSM-SG is a mathematical proof of this conclusion.

$$T = \frac{N_A^2}{S_W} \frac{h v_c (R_C + r_p)^3 L_{PC}^2}{2c R_C r_e R_{ig}} \frac{\mu_e}{\mu_n} = 2.6758K \tag{8}$$

**Other estimated CL space parameters:**
**CL node distance** (at xyz axes) ~ $1.0975 \times 10^{-20}$ (m),
**NRM (resonance) frequency**: $1.0926 \times 10^{29}$ (Hz)
**SPM frequency** = Compton's frequency (known): $1.2356 \times 10^{20}$ (Hz)
**ZPE-S**=$1.373 \times 10^{26}$ (J) – <u>Static Zero Point Eenergy of space (hidden energy of non EM type – a primary source of the nuclear energy (BSM, Chapter 5)</u>

Using the particle data and the derived mass equation, the internal structure of the proton and neutron is identified, as shown in Fig 5. The calculated dimensions are verified by analysis of atoms connected in molecules and by comparison with experimentally obtained bond lengths.
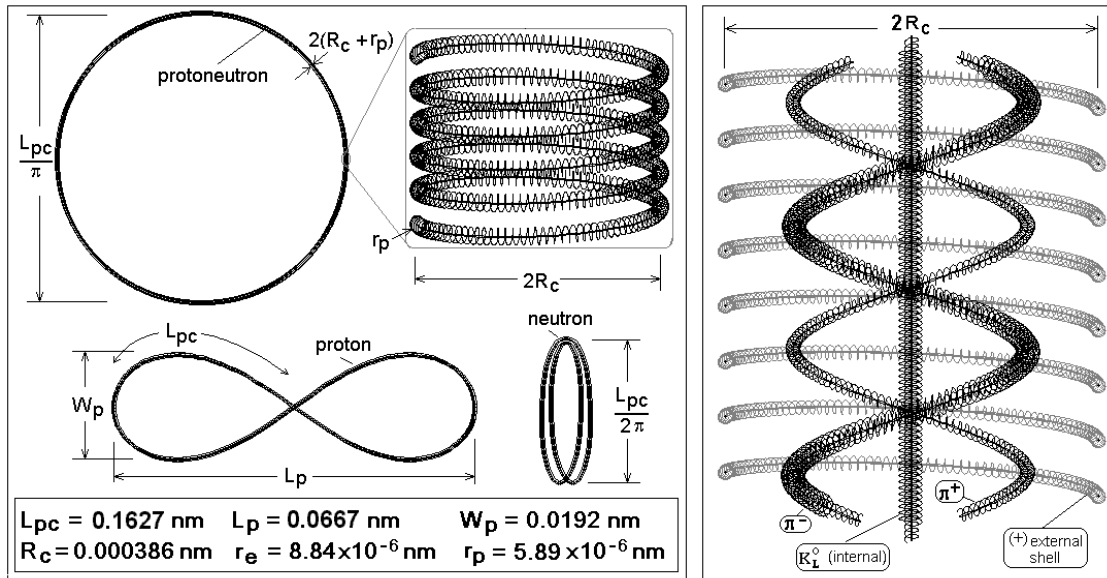
**Fig. 5.** Overall shape and internal structure of the proton and neutron with calculated dimensions

The protoneutron with the shape of the torus is unstable in CL space. The proton has the same structure but is twisted in a shape of 8, as shown in Fig. 5 so it is stable. The neutron has the same structure but is almost double folded, as shown in Fig. 5 and it is more stable when it is over the proton forming a deuterium, as shown in Fig. 6. The CL space modulation from the proton (CL node dynamics) appears as a charge, but for the neutron it is compensated in the far field due to the symmetry of its internal structure. The neutron's charge appears "locked" in proximity, but it provides a small magnetic field, when in motion. **This is the reason for the magnetic moment of the neutron.** Fig. 6 shows the spatial arrangement of the protons and neutrons in the atomic nuclei.
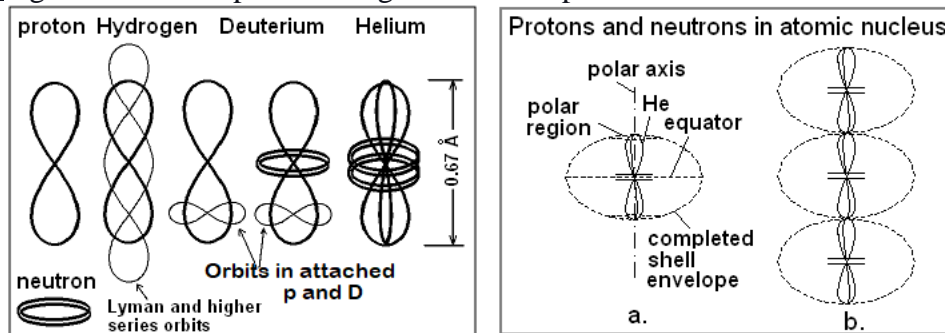


Fig. 6. Protons and neutrons arrangement in atomic nuclei

The unveiled nuclear structures of stable elements of the Mendeleev Periodic Table are presented in the Atlas of Atomic Nuclear Structures – Appendix A of the BSM-SG book [17,31]. The protons and neutrons are shown by symbols for simplifying the drawings, but 2D projections for each of them can be made as illustrated in Fig. 7. For a neutral atom each proton has own bound electron, so the positions of the electron quantum orbits are completely defined by the nuclear structure. The atomic nuclei are in fact slightly twisted due to the twisted 3D overall shape of the proton. This feature forces the moving single proton, neutron, electron, and atoms to rotate that defines the Broglie wavelength.
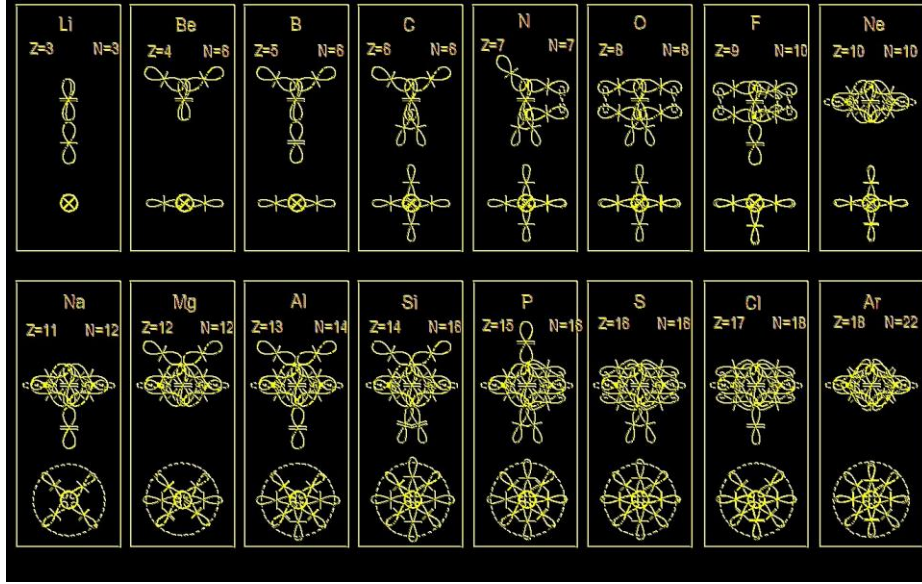
Fig. 7. Two rows of the Periodic table. The unbonded free ends of the deuterons (or protons) define the primary valence of the element. At noble gases they are bonded by the strong SG forces and excluded from chemical valences.
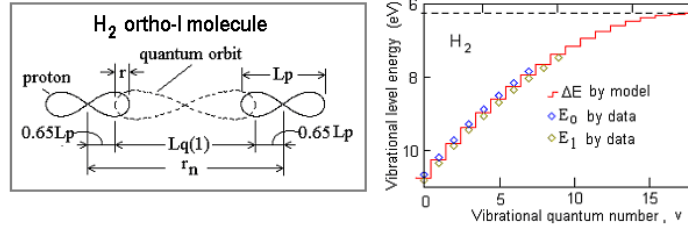


Fig. 8. A physical model of the $H_2$ – ortho molecule

The parameters of $H_2$ molecule (shown in Fig. 8) were obtained by using some optical and photoelectron spectra. It permitted the derivation of Eq. (9) for vibrational levels, plotted in Fig. 7 together with levels from the optical spectrum and obtaining the value of one important factor of the SG law denoted as $C_{SG}$ (Chapter 9 of BSM-SG). $H_2$– ortho system usually participates in chemical bonds between atoms.

$$E_V = \frac{C_{SG}}{q[[L_q(1)(1-\alpha^4\pi\Delta^2)]+0.6455L_p]^2} - \frac{2E_q}{q} - \frac{2E_k}{q} \qquad (9)$$

$$C_{SG} = G_0 m_0{}^2 = (2h\nu_c + h\nu_c\alpha^2)(L_q(1)+06455L_p)^2 = 5.2651\times10^{-33} \qquad (10)$$

$$C_{SG}/Gmp^2 = 2.82\times10^{31} \qquad (11)$$

where: $q$ –electron charge, $L_q(1)$ –quantum orbit length for electron velocity of 13.6 eV, $L_p$ – proton length, $\Delta$ - vibration level, $E_q$ = 511 KeV, $E_k$ – electron kinetic energy, $\nu_c$ – Compton frequency, $\alpha$ - fine structure constant, $G_{SG}$ – SG gravitational constant, $m_0$ – SG mass of the proton (also neutron).
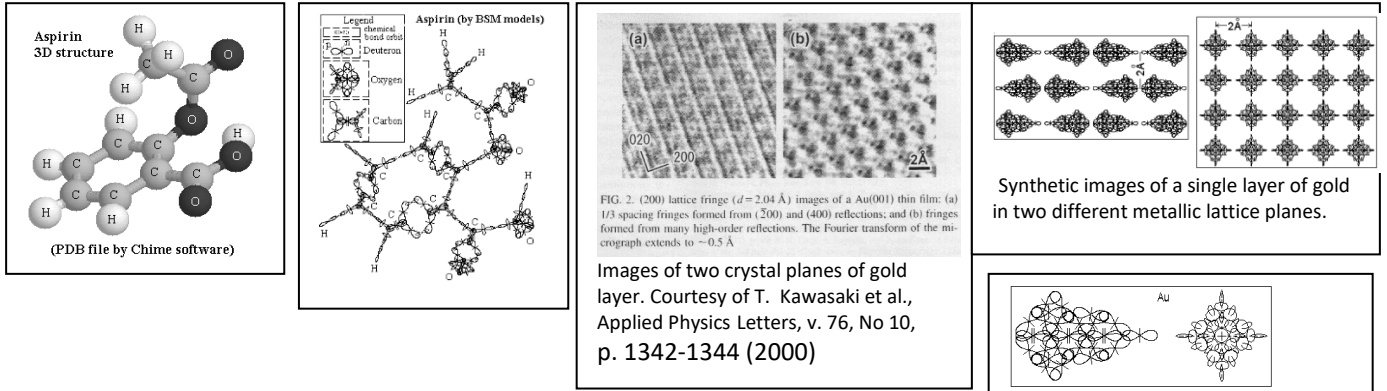
The ratio (11) shows that the FPs and their formations are enormously denser than the atomic matter. $C_{SG}$ factor is verified by calculating of the binding energy between the proton and neutron in the Deuterium (Chapter 6 of BSM-SG, p. 6-52). Using a simplified approximated model the calculated binding energy is 2.145 (MeV), which is quite closer to the experimentally obtained one 2.2245 (MeV).

The analysis and the derived structure of simple molecules indicate that the $H_2$ – ortho molecule participate as a chemical bond system in the molecules, having vibrational rotational spectra. An equation similar as (9) was derived also for $D_2$ molecule, which is a more common system in the chemical bonds. Then a universal expression (11) for internuclear distance, $r_n$, is derived for simple diatomic molecules. In &9.75.D (Chapter 9 pf BSM) it is shown that the real vibrational range is negligible in comparison to the internuclear distance $r_n$, due to the involved inverse cubic SG law (this has been irresolvable discrepancy between the Quantum Mechanical models and the observations).
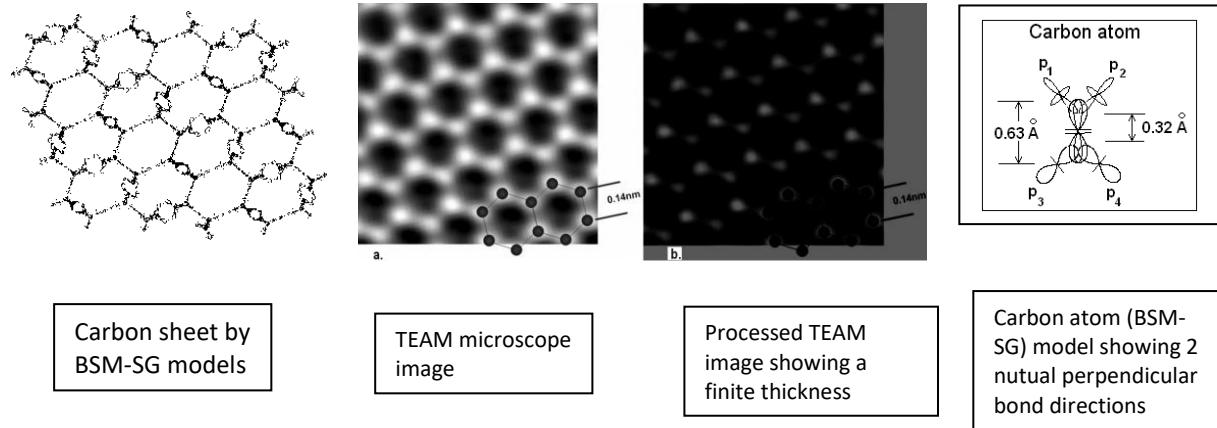
$$r_n = (A-p)[(2\alpha C_{SG})/(pB_{D2}(n))]^{1/2} \qquad (12)$$

where: A - mass in atomic mass unit (per one atom), $p$ – number of protons involved in the chemical bond (per one atom), $n$ – subharmonic quantum number of the orbit, $B_{D2}$ – energy of $D_2$ bonding system; $\alpha$ - fine structure constant

## Examples of BSM-SG atomic models for complex molecules and nanostructures



Aspirin 3D structure

(PDB file by Chime software)



Aspirin (by BSM models)



FIG. 2. (200) lattice fringe (d = 2.04 Å) images of a Au(001) thin film: (a) 1/3 spacing fringes formed from (200) and (400) reflections; and (b) fringes formed from many high-order reflections. The Fourier transform of the micrograph extends to ~0.5 Å

Images of two crystal planes of gold layer. Courtesy of T. Kawasaki et al., Applied Physics Letters, v. 76, No 10, p. 1342-1344 (2000)



Synthetic images of a single layer of gold in two different metallic lattice planes.



## Application of BSM-SG atomic models in modeling and analysis of nanostructures



Carbon sheet by BSM-SG models



TEAM microscope image



Processed TEAM image showing a finite thickness



Carbon atom (BSM-SG) model showing 2 nutual perpendicular bond directions

### Inertia beyond the Newton's first and second laws (Section 10.4.1. to 10.4.6 in Chapter 10 of BSM)

The CL node flexibility allows it to be partly folded and deviated when the electron (and any elementary particle) moves through the CL space. Multiplying Eq. (6) by the volume of the electron's structure we obtain

$$\vec{E}_{IFM} = P_p V_e = h v_c \alpha \vec{\upsilon} \ [J] \text{ - for a moving electron} \tag{13}$$

The vector $E_{IFM}$, called an Inertial Force Moment, allows estimating the deviation energy of the folded CL nodes, displaced from their normal positions at velocity $\upsilon$. It can be scaled for a moving proton (neutron) using the volume ratio between FOHSs of electron and proton (equal to their mass ratio). Eq. (14) is valid for a moving proton (neutron), while Eq. (15) for a moving atom with an atomic number A (u – is atomic mass unit)

$$\vec{E}_{IFM} = (m_p c \alpha) \vec{\upsilon} \text{ - for a moving proton;} \quad \vec{E}_{IFM} = (m_n c \alpha) \vec{\upsilon} \text{ - for a moving neutron} \tag{14}$$

$$\vec{E}_{IFM} = (c \alpha A u) \vec{\upsilon} \text{ - for a moving atom} \tag{15}$$

# Total energy balance of the moving macrobody through the Aether (Cosmic Lattice)

(Section 10.6 of Chapter 10 of BSM-SG)

Concidering the definition for a folding the force moment of a folding CL node we have $E_{IFM} = \alpha c m \upsilon$. Then change of the force moment for a particle with mass m in a free fall at acceleration $g$ per unite time is:

$$\Delta E_{IFM} = \alpha c m g \quad [J/s] \tag{17.a}$$

Let us consider the gravitational potential of a body at distance R from the Earth center. It is given by equation

$U_G = G \dfrac{Mm}{R}$ where: G - gravitational constant, M – mass of celestial body. m – mass of the falling body,

R – distance from the celestial body center. The acceleration due to gravity at that level is $g = G \dfrac{M}{R^2}$ and using

the Newton second law the acceleration force is $F = mg$. Then substituting denominator by Eq. (17.a) for the case of moving electron with mass $m_e$ we obtain the ratio

$$U_G \Big/ \Delta E_{IFM} = \frac{1}{\alpha c} R \quad [s] \tag{17.b}$$

We see that the dimension of Eq. (17.b) is time. Let us solve for distance R for a Compton's time. We obtain $R = \alpha c / v_c = 1.7706 \times 10^{-14} (m) \approx s_e = 2r_e$, where $\nu$ - is the Compton frequency [1/s]

Amazingly this value is quite close to the small radius of electron that was derived in Chapter 3, $2r_2 = 1.7685 \times 10^{-14} \quad (m)$

**Conclusion:** The **CL nodes folds and deviate** around the smaller electron radius $r_e$ - an indication of its **inertial interaction** with the CL space. The derived result is transferable to any elementary particle, by normalizing their mass to the mass of the electron.

We see that the mass *m* persists in $U_G$ and $\Delta E_{IFM}$ but no in their ratio. Therefore we may use this feature for analysis of their ratio for massive objects like planets and satellite. For convenience we denote this ratio as $K_E$.

$$K_E = U_G \Big/ \Delta E_{IFM} \tag{17.c}$$

## Unvealing the effect of gravitational pressure on the internal volume of massive celectial objects

For astronomicak body with a spin rotation, the falling body near the solid surface will get rotational energy that should decrease $U_G$. If assuming that unit mass of atmosphere (1 kg) is uniformly distributed as a thin shell at radius $R_v$ the rotation energy is

$$E_R = \frac{1}{2} I \omega^2, \text{ where } I = \tfrac{2}{3} m R_V^2 - \tfrac{1}{2} R_V^2$$

Then for a real astronomical body (planet or moon) the ratio $k_E$ becomes $\quad k_E = \dfrac{U_G - E_R}{\Delta E_{IFM}}$

Table 1 shows the planetary data sheets about the planets and moons of the solar system provided by NASA [30], (publicly available in year 2000). Using the table data the ratio $k_E$ was estimated. For this purpose the volumetric radius $R_V$ of the solid surface was used. For estimation of $\Delta E_{IFM}$, the surface gravity from the "fact data sheet" was used if it is available. Otherwise it was calculated by Eq. (17.a) where for mass, *m*, the planet (satellite) mass is used. The rotational energy of thin layer of atmosphere for the planets of the solar system is quite small so the parameter $E_R$ was ignored. Then the factor $K_E$ given by Eq. (17.c) was used.

$$K_E = U_G \Big/ \Delta E_{IFM} \tag{17.c}$$

Table 1.　　　　Planet (moon) data

| No Planet (moon) | M x $10^{23}$ (kg) | $R_v$ (km) | g (m²/s) | $T_{sid}$ (hr) | $K_E$ |
|---|---|---|---|---|---|
| 1. Nereid | 0.0002 | 170 | | | 0.077 |
| 2. Vesta | 0.000301 | 265 | | | 0.121 |
| 3. Umbriel | 0.0117 | 584.7 | | | 0.267 |
| 4. Charon | 0.019 | 593 | | | 0.27 |
| 5. Oberon | 0.0301 | 761.4 | | | 0.348 |
| 6. Titania | 0.0352 | 788.9 | | | 0.36 |
| 7. Pluto | 0.125 | 1195 | | 153.3 | 0.546 |
| 8. Triton | 0.2147 | 1352.6 | | 141 | 0.618 |
| 9. Europa | 0.4797 | 1569 | | 85.2 | 0.706 |
| 10. Moon | 0.7349 | 1737.4 | 1.62 | 655.7 | 0.796 |
| 11. Io | 0.8933 | 1815 | | 42.48 | 0.837 |
| 12. Calisto | 1.076 | 2403 | | 400.5 | 1.1 |
| 13. Titan | 1.345 | 2575 | | | 1.173 |
| 14. Ganimede | 1.482 | 2634 | | 171.6 | 1.21 |
| 15. Mercury | 3.302 | 2439.7 | 3.7 | 1407 | 1.11 |
| 16. Mars | 6.418 | 3390 | 3.69 | 24.62 | 1.562 |
| 17. Venus | 48.685 | 6051.8 | 8.87 | 5832 | 2.766 |
| 18. Earth | 59.736 | 6371 | 9.78 | 23.934 | 2.92 |

Fig. 9 shows a plot of Eq. (17.c) as a function of mean volumetric radius of the solar planets and moons, denoted by numbers. All points lie on the theoretical line with a slop $\frac{1}{\alpha c}$. **This is an amazing signature that the fine structure constant participate in the complex dynamics of the celestial objects**. However, we observe additionally one interesting anomaly. The planet M**ercury (number 15) appears in a reversed order in respect to the main trend.**
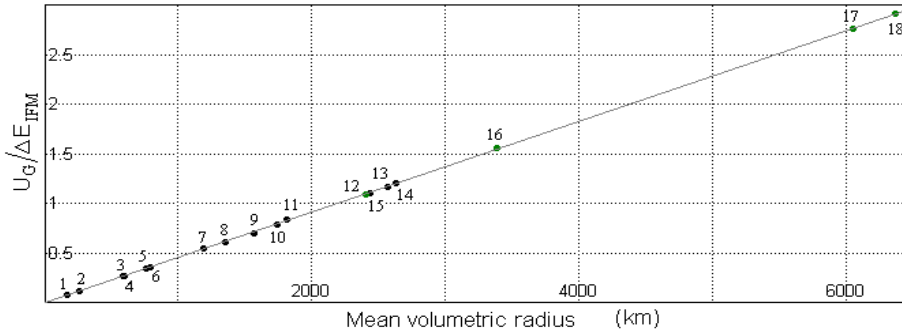


Fig. 9. Plot of Eq. (15) for solar planets and moons



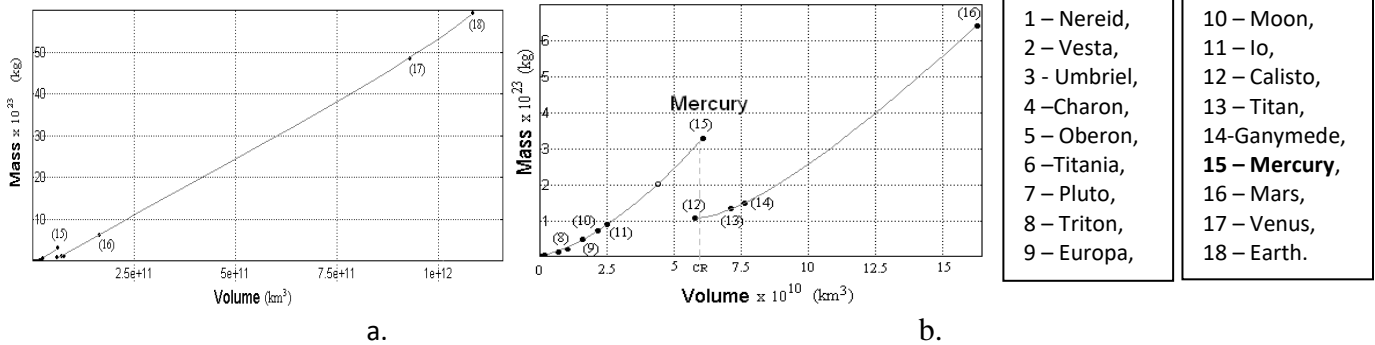| 1 – Nereid, | 10 – Moon, |
|---|---|
| 2 – Vesta, | 11 – Io, |
| 3 - Umbriel, | 12 – Calisto, |
| 4 –Charon, | 13 – Titan, |
| 5 – Oberon, | 14-Ganimede, |
| 6 –Titania, | **15 – Mercury**, |
| 7 – Pluto, | 16 – Mars, |
| 8 – Triton, | 17 – Venus, |
| 9 – Europa, | 18 – Earth. |

a.　　　　　　　　　　　　　　　　b.

Fig. 10. Planetary and moon masses versus their volumes. a. – normal plot; b. – expanded plot.

Investigating the observed anomaly we made a plot of mass of the celestial object versus the volume, as shown in Fig. 10. The anomaly is also evident, especially in the expanded plot.

$M_{CR} = 2.189 \times 10^{23}$  $(kg)$   - critical mass value

Amazingly the observed anomaly coincides with appearance of a magnetic field of the planets and satellites with masses greater than the critical mass $M_{CR}$.

The analysis permited to **formulation of  the following hypothesis:** The increased mass pressure leads to breaking the structures of protons and neutrons to straight helical structures. They become like the kaon and pions helical structures but stratelined as a bundle core. This bundle core obtains an enormouse matter density in comparison to the atomic matter, **while at the same time it possesses s super-strong anisotropic SG field at 180 degree. This bundle structure is behind the magnetic field of celestial bodies with a mass above some threshold level $M_{CR}$. Thiese predicted features are in excellent agreement with the cosmological observations leading to formation of pulsars. Many astronomical observations of supernovae show strong jets at 180 degrees. More details on mentioned analysis are available in Chapters 10&12 of BSM-SG.**

## Inferred connection between the fine structure constant and the gravitational constant

The experimentally determined fine structure constant, $\alpha$, is observed in experiments in different fields of physics and expecially in particle physics, spectroscopy, and the properties of electron. Despite it was estimated by a great accuracy this dimensionless constant bothered the mind of many famose scientists. The The BSM-SG theory unveils that the fine structure constant is a specific vibration mode of the Primary Tetrahedron, illustrated in Fig. 1, a.  It is dimensionless because it appears as a number of cycles between two specific positions of the pressessional vibrational mode of the Primary Tetrahedron. Its vibrational mode similar like the vibration of the CL node, but the number of sub-cycles is much smaller. Due to the different strength of the restoring forces along the two sets (xyz and abcd) axes of the CL node and the asymmetry between them, the single NRM cycle is an open 3D curve. If the hodograph of the NRM vector circumscribes a closed 3D surface for 137 NRM cycles plus a small fraction, one obtains the empirical formula (20) matching accurately the value of $\alpha$ given by CODATA 98 (See section 12.A.5.3 Chapter 12 of BSM-SG, p. 12-16).

$$\alpha = 2/[(n^2 + 2\pi^2)^{1/2} + n] = 7.29735194 \times 10^{-3} \tag{20}$$

$\alpha = 7.2973525 \times 10^{-3}$   - experimental value by CODATA 98

Since the fine structure constant is a dynamical feature of the primary Tetrahedron it is embedded in all next levels of particle formation so its signature persists in many properties of the elementary particles and material objects. The BSM-SG theory obtains for the first time a relationship between the fine structure constant and the gravitational constant as shown below (see section 10.6.2.A, Chapter 10 of BSM-SG).

If a planet with a mass *Mp* is in a circular orbit with a radius *r* around a star with a  mass $M_S$ the gravitational attraction is equal to the centripetal acceleration. The tangential velocity is $\upsilon = \sqrt{GM_S/r}$ . The energy ratio between the inertial force moment (of the folded CL nodes) and the kinetic energy of the planet is given by the expression

$$\frac{E_{IFM}}{E_K} = \frac{\alpha c M_p \upsilon}{0.5 M_p \upsilon^2} = \frac{2\alpha c}{\sqrt{GM_S}} \sqrt{r} \tag{18}$$

Squaring the expression (18) we get

$$\left[\frac{E_{IFM}}{E_K}\right]^2 = \frac{4\alpha^2 c^2}{GM_S} r = C_E r \tag{19}$$

Where:       $C_E = \dfrac{4\alpha^2 c^2}{GM_S}$ (19.a)

For a solar mass $M_S = 1.9891 \times 10^{30} (kg)$, one obtains the factor $C_E = 1.44238 \times 10^{-7}$.

Table 2 shows the planetary data provided by NASA.

Table 2.    Planetary data  by NASA

| No | $M_P$ x $10^{23}$ [kg] | $\upsilon$ (mean) [km/sec] | d (mean) [au] | $\rho$ (mean) [kg/m$^3$] |
|---|---|---|---|---|
| 1 Mercury | 3.302 | 47.87 | 0.387 | 5427 |
| 2 Venus | 48.685 | 35.02 | 0.723 | 5243 |
| 3 Earth | 59.736 | 29.78 | 1 | 5515 |
| 4 Mars | 6.418 | 24.13 | 1.524 | 3933 |
| 5 Jupiter | 18986 | 13.07 | 5.203 | 1326 |
| 6 Saturn | 5684.6 | 9.69 | 9.539 | 687.26 |
| 7 Uranus | 868.3 | 6.81 | 19.18 | 1270 |
| 8 Neptune | 1024.3 | 5.43 | 30.06 | 1638 |
| 9 Pluto | 0.125 | 4.72 | 39.53 | 1750 |

$\upsilon$ - mean velocity
d – mean distance in astronomical units
$\rho$ - mean density

The calculated parameters $E_{IMF}$ and $E_K$ from the table excibit quite large variation for different planets (a few orders), although the square values of their ratio given by Eq. 19 exhibits a perfectly linear dependence on their distance from the Sun. Fig. 12 shows a plot of $[E_{IFM}/E_K]^2$ versus the mean orbital radius $r$ for the solar planets. The slop of the fitted line gives a data value of $C_E$, which differs only by 0.06% from the theoretical one, given by Eq. (19.a).



Solar system planets.
----------------------------
1.    Mercury
2.    Venus
3.    Earth
4.    Mars
5.    Jupiter
6.    Saturn
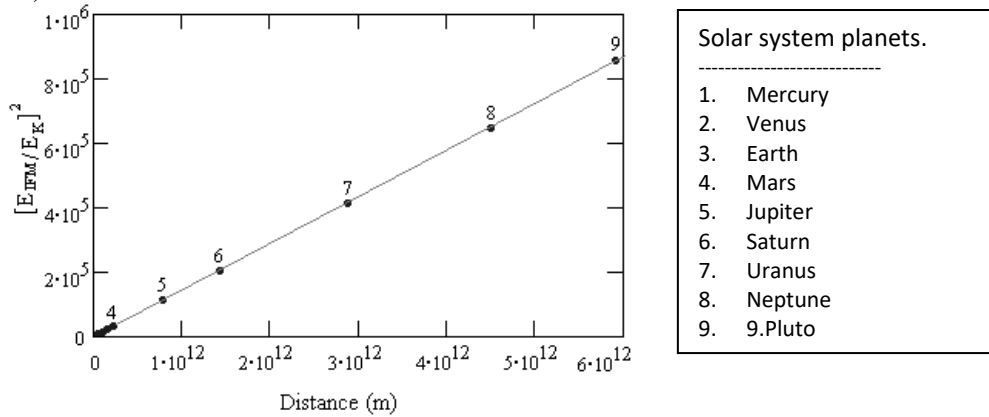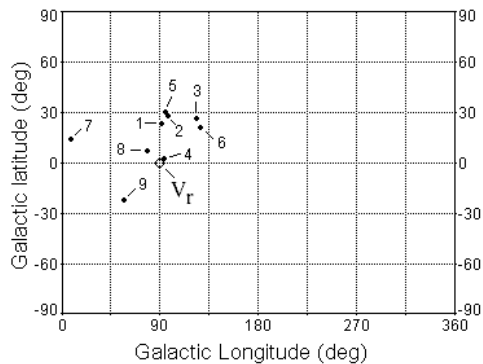7.    Uranus
8.    Neptune
9.    9.Pluto

Fig. 12 $[E_{IFM}/E_K]^2$ versus the mean orbital radius $r$ for the solar planets.

**Conclusions:**

The expressions (18) and (19) and corresponding plots indicate that the **fine structure constant ($\alpha$) plays an important role in the inertial interactions**.



According to the presented physical model, $\alpha$ should be a stable constant, while the gravitational constant G may slightly vary, depending on the mass of the astronomical body. This is in good agreement with the BSM-SG interpretation of the General Relativity, and might help understanding some local variations of G and some problems in astronomy about some peculiar motions of distant star formations. According to Eq. (19), the ratio between $P_S$ (related to the mass) and $P_P$ (related to the dynamics of any object - particle, atom, molecule and solid object) has a preferable value defined by the fine structure constant. When regarded as an optimal tendency, this ratio might have a signature even in the galactic rotational curves and the evolution of the galaxies from $S_0$

13

to $S_B$ or Sc branch. This conclusion comes from the BSM-SG analysis of the galactic rotational curves for different types of galaxies provided by Rubin et al. [27] and other researchers.

One indication of inertial interactions between the rotating massive object and CL space is the preferable orientation of the polar axes of the solar planets in respect to the galactic rotation of the solar system, as shown in Fig. 13. The effect is consistent with the inertial mass anomaly observed in spinning gyroscopes [28].

Fig. 13. Solar vector $V_r$ and North polar axes of the solar system planets in galactic coordinates (data from planetary datasheets). 1- Mercury, 2 – Venus, 3 – Earth, 4 – Mars, 5, Mars, 6 – Saturn, 7, Uranus, 8 – Neptun, 9 – Pluto

## A new vision about the Universe (Chapter 12 of BSM-SG)

The individual galaxies have their own cycle of active life (observable) and hidden not observable phases, where the matter recycle to lower formations and crystallization of new elementary particles takes place. The transition events between the observable and hidden phases are the galactic collapse and galactic birth, which have detectable signatures – the observable Gamma Ray Bursts (GRB). Some galactic matter, escaping the collapse, forms the Globular Clusters and "Irregular galaxies", such as Sagittarius. In the formation of the sub-elementary particles denited as prisms, all galactic matter (detectable during the galactic active life) participates. Since the total galactic mass of the fiferant galaxies is different, prisms from their formations will have a small variation of their length to radius ratio. Then a photon emitted and detected in one and a same galactic space will not have a cosmological redshift (the environment preserve the optimal quantum interactions). However, a photon passing through different galactic spaces will exibit a small energy loss due to refurbishing of its wavetrain in the boundary zones between the galaxies. The observable effect is a galactic readshift, which is not of Doppler origin. If expressing the difference between two galactic spaces as an average quasirefractive index, $\tilde{n}$, the ratio between the observed and emitted wavelength of the photon is

$\lambda_i / \lambda_0 = (\tilde{n})^N$   which leads to the expression

$$(\tilde{n})^N = z + 1 \qquad (24)$$

where: z – is the cosmological redshift from N crossed galactic boundaries

One detectable signature of this phenomenon is the Lyman Alpha Forest, providing an estimate of the number of crossed boundaries. Then the new corrected distance to a galaxy with a redshift of z is given by

$$r = \frac{c^2 \ln(\tilde{n})^N}{\tilde{L}} \int_0^z \frac{x}{\ln(1+x)} dx \qquad (25)$$

where: $\tilde{n}$ - is determined from the mean density of the Lyman alpha forest lines for signal emitted by a distant quasar,

$\tilde{L}$ - an average distance between the neighboring galaxies, $H_0$ – Hubble constant, $c$ – velocity of light

Figure 14 shows a Hubble plot from experimental data for z up to 1.75 [28], while Fig. 15 shows the theoretical plot of Eq. 20, normalized to the constant $(c^2 \ln(\tilde{n}) / \tilde{L}_0 H_0)$
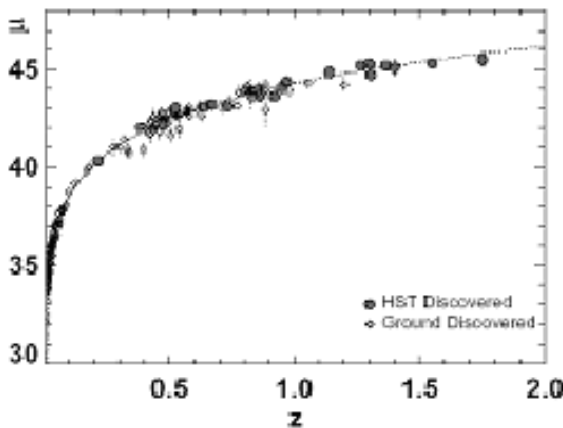


Fig. 14                                    Fig. 15
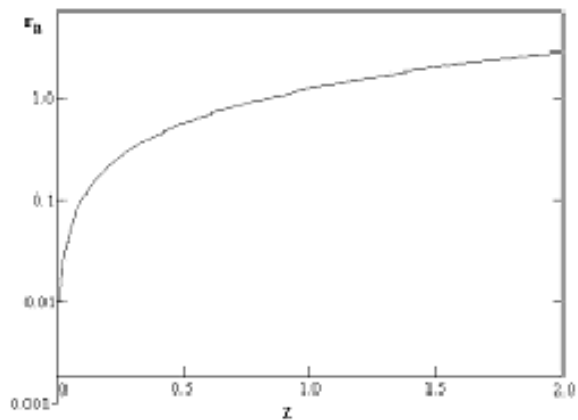
Observations of Huble plot at larzer redshifts show departure from the trend predicted by Big Bang theory. However they agree with the trend of the theoretical plot of BSM-SG theory for a stationary nonexpanding Universe, where the redshift is not of Doppler, but by of cosmological origin. This is demonstrated by the plots in log-log scale shown in Fig. 16 and Fig. 17. **The trend for higher redshifts deviates up from the straight line, so the redshift is of cosmological origin** (see the detailed analysis in Chapter 12).
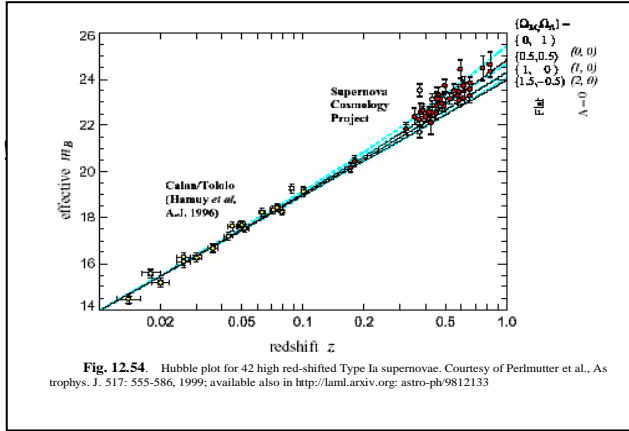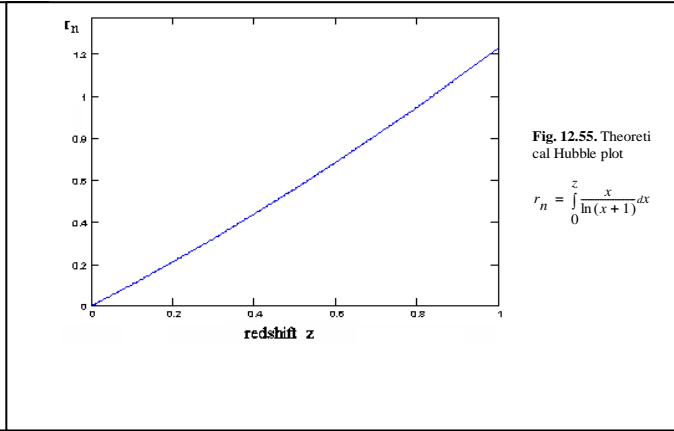


**Fig. 12.54**. Hubble plot for 42 high red-shifted Type Ia supernovae. Courtesy of Perlmutter et al., Astrophys. J. 517: 555-586, 1999; available also in http://laml.arxiv.org: astro-ph/9812133

**Fig. 12.55.** Theoretical Hubble plot

$$r_n = \int_0^z \frac{x}{\ln(x+1)} dx$$

|  |  |
|---|---|
| Fig. 16 | Fig.17 |

The mass is a parameter of a structural formations from indestructible Fundamental Particles, so it is not equivalent to matter. Consequently, annihilation or creation of matter (Fundamental Particles) is impossible.

The new concept of the physical vacuum leads to important predictions, discussed in Chapter 13 of BSM-SG. The most important of them are: (1). Unveiling a hidden space energy of non EM type, which is the primary source of the nuclear energy, (2) Predicting a new method for supercomunication by using not well investigated so far longitudinal waves, (3) Predicting the possibility for control the gravitational and inertial mass of material object, by proper modulation of the physical vacuum parameters.

**Summary and conclusions: The new concept of the physical vacuum leads to a logically understandable physical models about space, time, matter, energy, gravitation, and quantum mechanical properties. It unveils a different picture about the microcosmos and Universe.**

- **The common origin of the observed world from micro to macro scale is explainable by a physical model of two indestructible Fundamental Particles with parameters associated to Palnck's scale and interactions governed by an inverse cubic law called a Law of Supergravitation**
- **The Supergravitational law is the most fundamental law in Universe.**
- **The physical vacuum contains underlying superfine material structure. It defines space-time, Quantum Mechanical, and Relativistic properties of the space and it is responsible for propagation of the Gravitational, Electrical and Magnetic fields.**
- **The fundamental laws of Physics are embedded in the superfine material structures of the physical vacuum and the elementary particles.**
- **The fine structure constant is embedded in the basic level of matter organization, while its signature is propagated in all upper levels.**
- **The galactic redshift is not of a Doppler type. The Universe is stationary.**
  - **Analysis of cosmological observations reveals that the galaxies possess their own cycle in which the elementary particles are formed at the hidden nonobservable phase of the cycle.**
- **The Galactic cycle is comprised of a visible active life and a hidden phase of matter recycling. The collapse or birth of a galaxy creates a strong detectable event known as the Gamma Ray Burst (GRB). It is a result of the stress in the underlying Aether structure interconnection with the**

neighboring galaxies. The Globular Clusters and some irregular galaxies (like Sagittarius) are remnants from the previous galactic life, which have escaped the collapse.

- **The space contains hidden (not EM type) energy, which is the primary source of the nuclear energy. Alternative methods for access to this energy are possible (Chapter 13 of BSM-SG).**
- **The Gravitational and inertial mass of a solid body could be changed by proper modulation of the vibrational properties of the underlying space structure – the Cosmic Lattice. This is – a promising opportunity for a new method of distant space travels (Chapter 13 of BSM-SG; more details are available in the author's book Field Propulsion by Control of Gravity [[8] ).**

## Online accessible publications of the author

https://www.helical-structures.org/  Author's page since 2001

http://earthcivilizationanduniverse.eu/ Society page since 2022

https://beyondmainstream.org/scientist/dr-stoyan-sarg/  Beyond Main Stream Science

https://www.amazon.com/stores/Stoyan-Sarg/author/B00J3F2A0Q  Stoyan Sarg central page

http://wiki.naturalphilosophy.org/index.php?title=Stoyan_Sarg  National Philosophy Alliance

https://philpeople.org/profiles/stoyan-sarg-sargoytchev on-line community for philosophers

http://vixra.org/author/Stoyan_Sarg - selected articles

https://www.gsjournal.net/Science-Journals-Papers/Author/1881/

https://independent.academia.edu/StoyanSargSargoytchev

https://brevets-patents.ic.gc.ca/opic-cipo/cpd/eng/patent/2638667/summary.html
     Patent Application "Method and apparatus for spacecraft propulsion"

https://helical-structures.org/Heliconstruct/table.html BSM-SG Periodic table of elements

https://www.foreignpolicyjournal.com/author/stoyan-sarg/  popular publications

http://arxiv.org/pdf/physics/0205052 First publication about BSM-SG

https://www.slideshare.net  search: Stoyan Sarg (slides from conference talks)

http://youtube.com/user/tenko45/videos  Youtube cannel of Stoyan Sarg

**SSE 2008 27th Annual Meeting Colorado. Videorecords placed by SSE**

https://www.youtube.com/watch?v=s5ypGrw5q1w  Gravito-inertial propulsion part 1

https://www.youtube.com/watch?v=ZOY2mPmZjvE Gravito-inertial propulsion part 2

https://www.youtube.com/watch?v=NT7eHuSYayc  Gravito-inertial propulsion part 3

**SSE-2012 31st Annual meeting Colorado Videorecords placed by SSE**

https://www.youtube.com/watch?v=S3gJp8rLHWg BSM and LENR part1 (2012)

https://www.youtube.com/watch?v=WQYXj07yf8g BSM and LENR part2 (2012)

https://www.youtube.com/watch?v=Di79FvZEMK0 BSM and LENR part3 (2012)

**Nanotek & Expo 2014 San Francisco**

https://www.youtube.com/watch?v=EUWVHa9kOoU Stoyan Sarg keynote talk

**Medical Nanotechnology, Osaka, Japan, 2017**

https://www.youtube.com/watch?v=W8A26MLwXLI Stoyan Sarg keynote talk

## References:

1. N. A. Zhuck et al, Quasars and the large-scale structure of the Universe, Spacetime & Sustance, v. 2 No. 5 (10), p.193-210, (2001)
2. J. C. Maxwell, *A Treatise on Electricity and Magnetism*, v. 2 (Dover Publications, N. Y. p. 493, (1954))
3. A. Einstein, *Sidelights on Relativity*, translated by G. Jeffery & W. Perrett, Methuen & Co. Ltd, London, (1922)
4. D. C. Miller, The Ether-Drift Experiment and Determination of  Absolute Motion of the Earth, Review of Modern Physics, 5, 203-242, (1933)
5. G. F. Smoot et al., Detection of Anisotropy in the Cosmic Blackbody Radiation, Physical Review Letters, 39, No 14, 898-901, (1977)
6. R. A. Muller, The Cosmic Background Radiation and the New Aether Drift, Scientific American, 238, 64, (1978)
7. S. Marinov, Measurement of the Laboratory's Absolute velocity, General Relativity and Gravitation, 12, 57-66, (1980)
8. Stoyan Sarg, *Feld propulsion by control of gravity, Theory and experiments*, (2009), ISBN13 978-1448693085
9. E. W. Silvertooth, Experimental detection of the ether, Speculations in Science and Technology, 10, No 1, 3-7, (1986)

10. Stoyan Sarg, https://www.gsjournal.net/Science-Journals/Essays/View/9908

11. C. Monstein and J. P. Wesley, Solar System Velocity from Muon Flux Anisotropy, Apeiron, 3, No. 2, 33-37, (1996)

12. R. T. Chill and Kirsty Kitto, Michelson-Morley Experiments Revisited and the Cosmic Background Radiation Preferred Frame, Apeiron, 10, No 2, 104-1017, (2003)

13. M. Consoli and E. Costanzo, From Classical to modern ether-drift experiments: the narrow window for a preferred frame, Physics Letters A, 333, 355-363, (2004), also arXiv:astro-ph/0601420 v. 2, (2006)

14. S. Sarg, Basic Structures of Matter (first edition 2002, second edition, 2002) electronic archives, National Library of Canada

15. S. Sarg, *Basic Structures of Matter – Supergravitation Unified Theory*, Trafford Publishing, Canada, 2006, ISBN 141208387-7 (www.trafford.com/06-01421).

16. S. Sarg, New approach for building of unified theory, http://lanl.arxiv.org/abs/physics/0205052 (May 2002)

17. S. Sarg © 2001, Atlas of Atomic Nuclear Structures, monograph, http://www.nlc-bnc.ca/amicus/index-e.html (April, 2002), (AMICUS No. 27106037); Canadiana: 2002007655X; ISBN: 0973051515, LC Class: QC794.6*; Dewey: 530.14/2 21

18. S. Sarg, Brief introduction to Basic Structures of Matter theory and derived atomic models, Journal of Theoretics (Extensive papers), January, 2003; http://www.journaloftheoretics.com

19. S. Sarg, Atlas of Atomic Nuclear Structures according to the Basic Structures of Matter Theory, Journal of Theoretics (Extensive papers, March, 2003); http://www.journaloftheoretics.com

20. S Sarg, Application of BSM atomic models for theoretical analysis of biomolecules (with three formulated hypotheses), Journal of Theoretics, May 2003; http://www.journaloftheoretics.com

21. S. Sarg, A Physical Model of the Electron according to the Basic Structures of Matter Hypothesis, Physics Essays, 16 No. 2, 180-195, (2003); http://www.physicsessays.com

22. S. Sarg, New vision about a controllable fusion reaction with efficient energy yield, ISBN 0973051523 , (AMICUS No 27276360), (2002)

23. S. Sarg, Basic Structure of Matter Hypothesis Based on an Alternative Concept of the Physical Vacuum (poster report), "Physics for the Third Millennium" Conference, organized by NASA, Huntsville Al, USA, 5-7 Apr 2005.

24. S. Sarg, Basic Structures of Matter Hypothesis Based on an Alternative Concept of the Physical Vacuum, 12th Annual conference of Natural Philosophy Alliances, 23-27 May 2005, Storrs, CT, USA.

25. S. Sarg, *Beyond the Visible Universe*, Helical Structures Press, Canada, 2004, ISBN 0973051531

26. A. I. Zakazchikov, The evolution of the vision about Ether, Proc. Of VIII International Scientific Conference, "Space, Time, Gravitation", 16-20 Aug 2004, St. Petersburg, Russia (p. 96-110)

27. Rubin et al., Rotation velocities of 16 Sa galaxies and a comparison of Sa, Sb and Sc rotation properties, Astrophysical Journal, 289, 81-104, (1985)

28. K. Gerber, R. Merritt and E. Delvers, Gyro Drop Experiment http://depalma.pair.com/gyrodrop.html

29. Stoyan Sarg, Basic Structures of Matter – Supergravitation Unified Theory Based on an Alternative Concept of the Physical Vacuum, Proceeding of IX International Scientific Conference, Space, Time, Gravitation, 7-11 Aug 2006, Sankt Pteresburg, Russia.

30. NASA fact data sheets about planets and moons. (http://nssdc.gsfc.nasa.gov./planetary/planettact.html)

31. Stoyan Sarg, Atlas of Nuclear Atomic Structures - Clickable Periodic Table of elements https://helical-structures.org/Heliconstruct/table.html

## Appendices:

Appendices A: (Extracted from BSN-SG theory)

      Atlas of Atomic Nuclear structures – Introduction (pages A3, A4)

      Atlas of Atomic Nuclear structures Part I (elementary particles)

      Atlas of Atomic Nuclear structures Part II: Nuclear build-up trend,

               and Clickables Periodic Table: link https://helical-structures.org/Heliconstruct/table.html

Appendix B: Periodic Table of elements according to BSM-SG

Appendix E: Derived equations

# Atlas of Atomic Nuclear Structures

**Abstract** The Atlas of Atomic Nuclear Structures (ANS) is one of the major output results of the Basic Structures of Matter (BSM) theory, based on an alternative concept of the physical vacuum. The atlas of ANS contains drawings illustrating the structure of the elementary particles and the atomic nuclei. While the unveiled physical structures of the elementary particles exhibit the same interaction energies as the Quantum Mechanical models, they permit revealing the spatial configurations of the atomic nuclei, the atoms and the molecules. The unveiled structural features allows to understand the cause of radioactivity. The proposed physical models could find applications in different fields, such as chemistry, nuclear reaction, nanotechnology and biomolecules.

## Tables of contents

### Table 1: Page location of the elements

| Z | Page | | Z | Page |
|---|---|---|---|---|
| 1 - 2 | II-1 | | 53 - 56 | II-11 |
| 3 - 7 | II-2 | | 57 - 61 | II-12 |
| 8 - 13 | II-3 | | 62 - 67 | II-13 |
| 14 - 18 | II-4 | | 68 - 72 | II-14 |
| 19 - 24 | II-5 | | 73 -78 | II-15 |
| 24 - 29 | II-6 | | 79 - 84 | II-16 |
| 30 - 35 | II-7 | | 85 - 89 | II-17 |
| 36 - 40 | II-8 | | 90 - 95 | II-18 |
| 41 - 46 | II-9 | | 96 - 101 | II-19 |
| 47 - 52 | II-10 | | 102-103 | II-20 |

Notes: The symbols used for notation of the protons and neutrons and their connections in the atomic nucleus are given in Page II-).

Notations:

 Z- number of protons in the nucleus
 N - number of neutrons in the nucleus

atomic mass

$^{12}C$
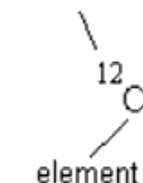
element

Element notation

**References:**

S. Sarg,  *Basic Structures of Matter*, monograph,  http://www.helical-structures.org,
 also in http://collection.nlc-bnc.ca/amicus/index-e.html (AMICUS No. 27105955), (first edition, 2002); second edition, 2005)

S. Sarg, New approach for building of unified theory about the Universe and some results,
 http://lanl.arxiv.org/abs/physics/0205052 (2002)

S. Sarg, Brief introduction to BSM theory and derived atomic models, Journal of Theoretics,
 http://www.journaloftheoretics.com/Links/Papers/Sarg.pdf

S. Sarg, A Physical Model of the Electron According to the Basic Structures of Matter Hypothesis, Physics Essays (An international journal dedicated to fundamental questions in Physics), v. 16, No. 2, 180-195, (2003)

# Introduction

The Atlas of Atomic Nuclear Structures (ANS) is one of the major output results of the Basic Structures of Matter (BSM) theory, based on an alternative concept of the physical vacuum. While the physical structures of the elementary particles obtained by analysis according to the BSM theory exhibit the same interaction energies as the Quantum Mechanical models, they allow unveiling the spatial configurations of the atomic nuclei, atoms and molecules. The unveiled structural features of the atomic nuclei provide explanation about the particular angular positions of the chemical bonds. Such features are in good agreement with the VSEPR model used in the chemistry. Number of other intrinsic features defined by the structural composition of the nuclei provides strong evidence that the proposed models are real physical atomic structures. The arguments for this claim are presented in the BSM theory and more particularly in Chapter 8. The proposed physical models allows understanding the radioactivity. They could be useful in different fields, such as chemistry, nuclear reactions, nanotechnology and biomolecules.

The atlas of ANS contains two parts. Part I illustrates the geometry and the internal structure of the basic atomic particles, built of helical structures. (The helical structures have common geometrical features. Their type and classification are shown in §2.7, Chapter 2 of BSM). Part II illustrates the three dimensional atomic nuclear structures of the elements in a range of $1 < Z < 103$, where Z is the number of protons in the nucleus. Only the stable isotopes given in the Periodic table are shown. In order to simplify the complex views of the nuclei they are shown as plane projections of symbols. For this purpose two types of symbols are used: symbols for hadron particles (proton, neutron and He nucleus) and symbols for the type of the nuclear bonding of the hadrons. The symbolic views contain the necessary information for presenting the real three-dimensional structures of the atomic nuclei by different sectional views. This is demonstrated in page 21 of the atlas, where nuclear sectional views of some selected elements are shown.

The rules according to which the protons and neutrons are arranged in shells in the nuclei are discussed in Chapter 8 of BSM. The trend of consecutive nuclear building by Z-number follows a shell structure that complies strictly with the row-column pattern of the Periodic table. The periodic law of Mendeleev appears to reflect not only the Z-number, but also the shell structure of the atomic nuclei. The latter becomes apparent in the BSM analysis. The protons (deuterons) shells get stable completion at column 18 (noble gases). The separate rows of the Lanthanides and the Actinides are characterised by a consecutive grow and completion of different shells. The nuclear structures of all stable elements (isotopes) possess a clearly identifiable polar axis of rotational symmetry. One or more He nuclear structures are always positioned along this axis. The most abundant sub-nuclear compositions are deuterons, tritium and protons. The strong SG forces hold them together, while the proximity E-fields play a role for their orientations. The identified different types of bonds are shown in the atlas by symbolic notations. For more details, see Chapter 8 of BSM. In the same Chapter, the conditions for instability of the short-lived isotopes are also discussed. They are partly apparent from the Atlas drawings - especially for the alpha decay. The growing limit for stable high Z-number elements is apparent from the shelf completion and the obtained nuclear shape.

The electronic orbits are not shown in the nuclear drawings, but their positions are defined by the spatial positions of the protons (or deuterons). The Hund's rules and the Pauli exclusion principle are both identifiable features related to the available positions and mutual orientations of the quantum orbits. The quantum velocity of the orbiting and oscillating electron, defines the length trace of any quantum orbit (see §3.12, Chapter 3; §7.4, Chapter 7 of BSM)
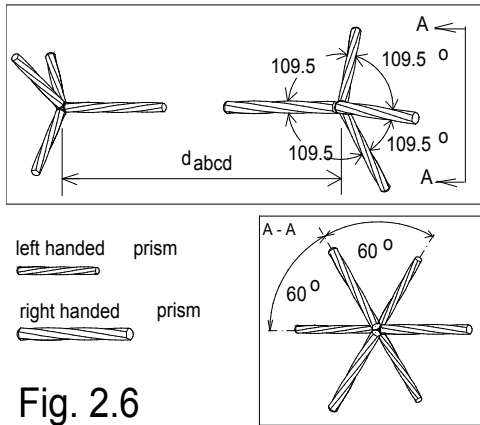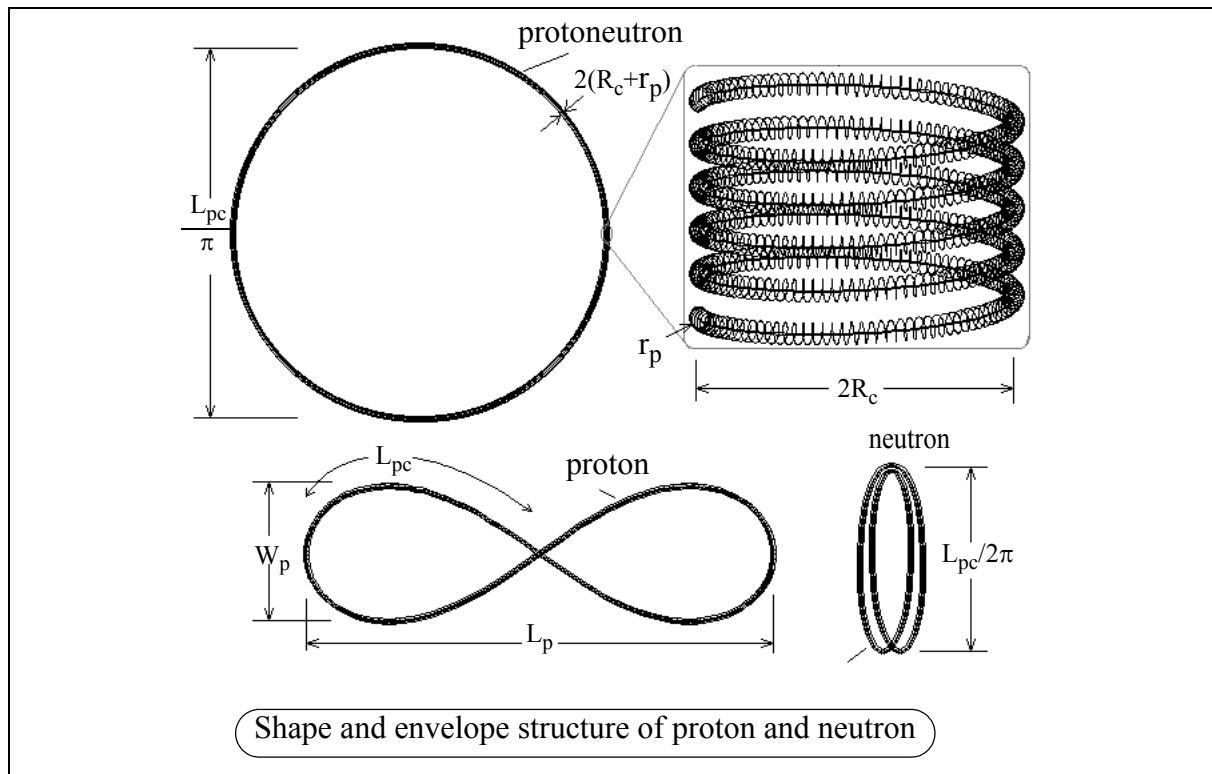
Fig. 2.6



Core node from prisms of same type
(building element of the helical structure)
Note: The twisted prisms model is used

Fig. 2.8.B



Electron structure geometrical parameters



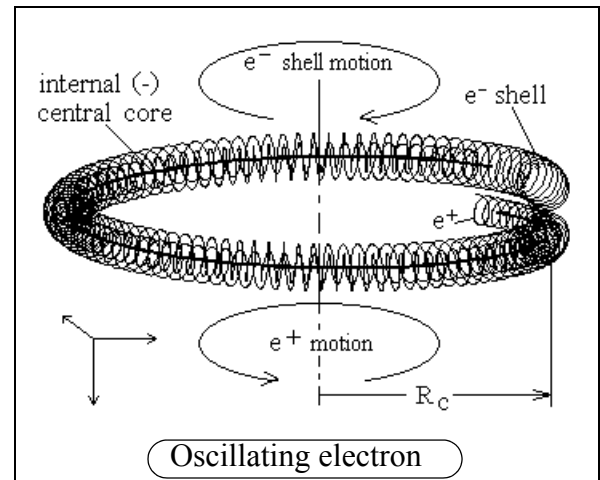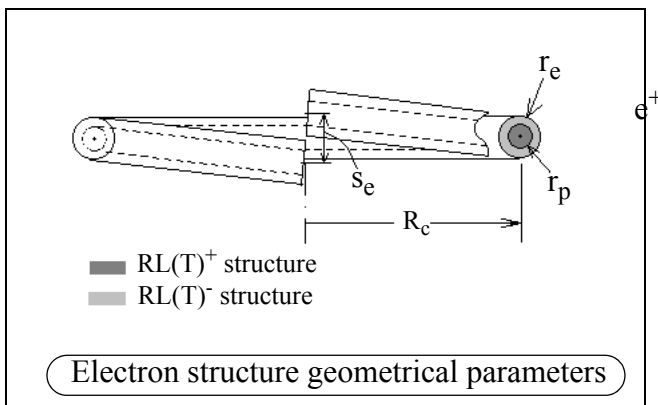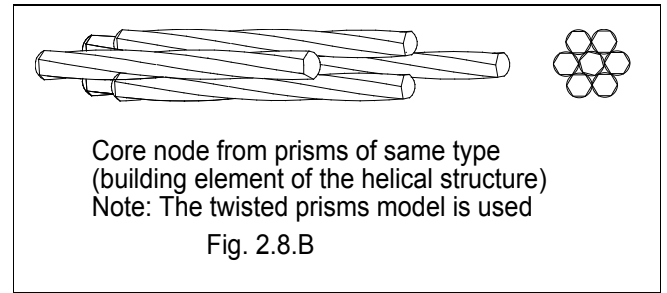Oscillating electron



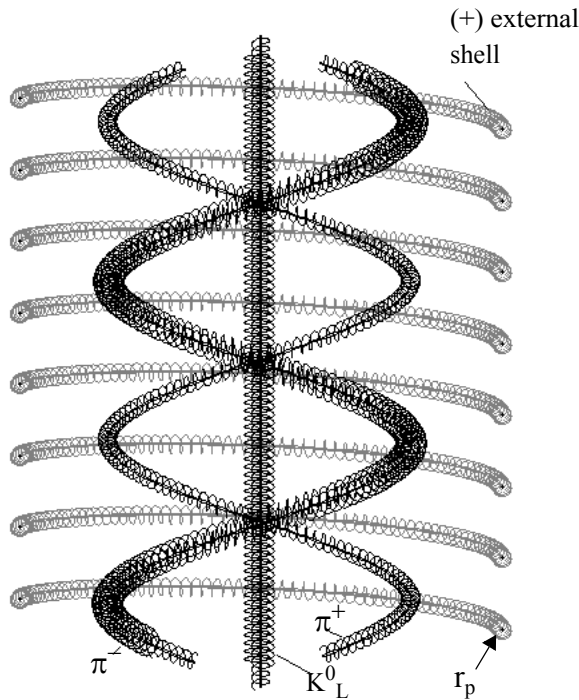Shape and envelope structure of proton and neutron

Fig. 2.15.B. Axial sectional view of proton (neutron) showing the external positive shell (envelope) and the internal elementary particles - pions and kaon. All of them are formed by helical structures possessing internal RL structures (not shown).



Fig. 2.16 Axial (a) and radial (b) section geometry of the internal RL structure of FOHS (not twisted). The real number of radial layers is large since the prism's length is much smaller than the boundary radius $r$.



Fig. 2.15.A. Radial sectional view of a proton (neutron) core with internal elementary particles and their internal RL structures. The RL structures are not twisted for the kaon, partly twisted for the pions and fully twisted for the external shell.



Fig. 2.29.E. Radial section of positive FOHS with twisted internal $RL(T)^+$ structure generating E-field in CL space. The radial section of the FOHS envelope core and the central core is formed of 7 prisms. $r_p$ - is a radius of the FOHS envelope.

Deuteron with Balmer series orbital
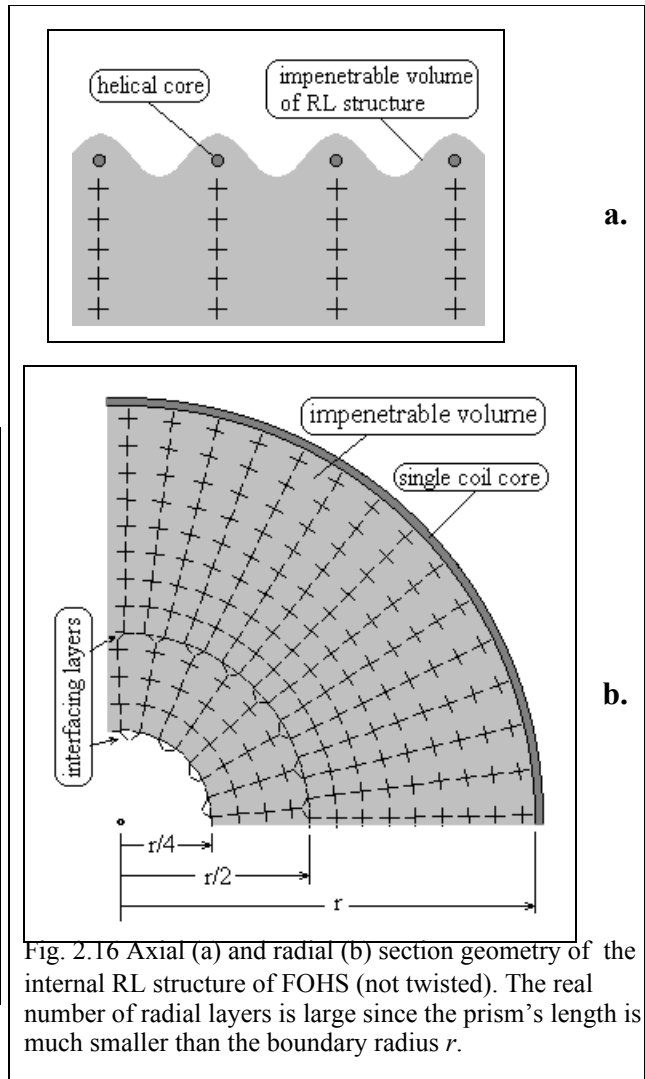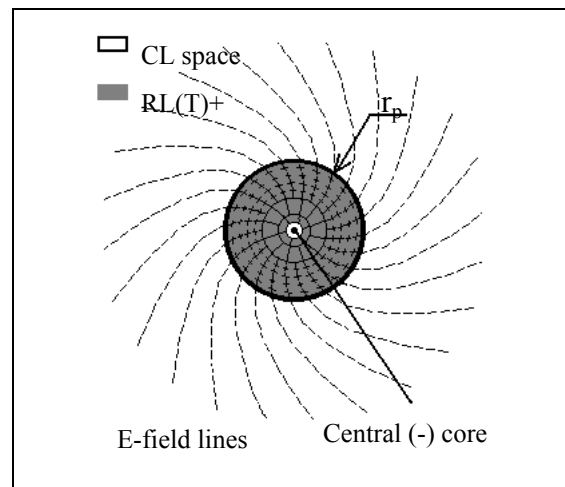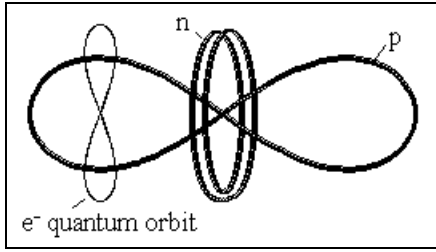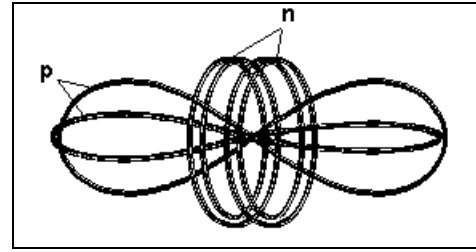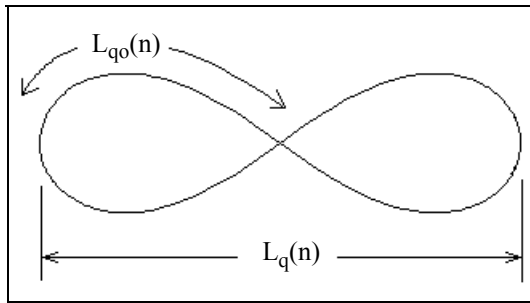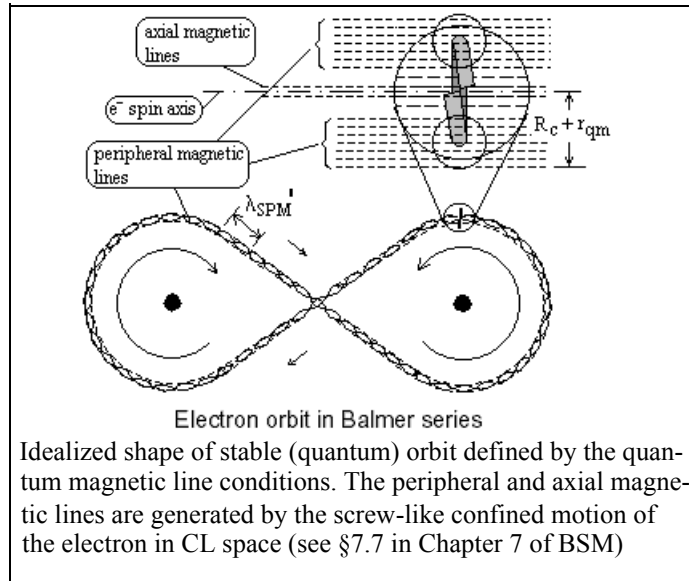


He nucleus

p - proton; n - neutron; e⁻ - electron



Simple quantum orbit (n - is the subharmonic number)



Electron orbit in Balmer series

Idealized shape of stable (quantum) orbit defined by the quantum magnetic line conditions. The peripheral and axial magnetic lines are generated by the screw-like confined motion of the electron in CL space (see §7.7 in Chapter 7 of BSM)

The equation of the quantum orbit trace length, $L_{qo}$ is derived in §3.12.3 (Chapter 3 of BSM).

$$L_{qo}(n) = \frac{2\pi a_o}{n} = \frac{\lambda_c}{\alpha n} \qquad (3.43.i)$$

where: $n$ is the subharmonic number of the quantum orbit; $\lambda_c$ - is the Compton wavelength; $\alpha$ - is the fine structure constant; $2\pi a_o$ - is the length of the boundary orbit ($a_o$ - is the Bohr model radius)

The shape of the orbit is defined by the proximity E-field of the proton. The most abundant quantum orbit has a shape of Hippoped curve with a parameter $a = \sqrt{3}$. Orbits of such shapes serve also as electronic bonds connecting the atoms in molecules (see Chapter 9 of BSM).

**The trace length $L_{qo}$ and the long axis length $L_q$ of the possible simple quantum orbits (formed by single quantum loops) are given in Table 1.**

**The estimated distance between the CL nodes in abcd axis is**: $d_{abcd} \approx 0.549 \times 10^{-20}$ (m).

**Table 1:**

| n | $L_{qo}$ [A] | $L_q$ [A] | e⁻ energy [eV] |
|---|---|---|---|
| 1 | 3.3249 | 1.3626 | 13.6 |
| 2 | 1.6625 | 0.6813 | 3.4 |
| 3 | 1.1083 | 0.4542 | 1.51 |
| 4 | 0.8312 | 0.3406 | 0.85 |
| 5 | 0.665 | 0.2725 | 0.544 |
| 6 | 0.5541 | 0.2271 | 0.3779 |

**The calculated geometrical parameters** of the stable atomic particles: proton, neutron, electron and positron are given in **Table 2**. The last reference column points to the BSM chapters, related to the calculations and cross validations of these parameters.

**Table 2:**

| Parameter | Value | | Description | Calculations and cross validations in: |
|---|---|---|---|---|
| $L_{PC}$ | 1.6277 | (A) | proton (neutron) core length | Chapters 5 and 6 |
| $L_P$ | 0.667 | (A) | proton length | Chapters 6, 7, 8, 9 |
| $W_P$ | 0.19253 | (A) | proton (neutron) width | Chapters 6, 7 ,8 ,9 |
| $r_e$ | 8.8428E-15 | (m) | small radius of electron | Chapters 3, 4, 6 |
| $s_e$ | 1.7706E-14 | (m) | electron( positron) step | Chapter 3 |
| $r_p$ | 5.8952E-15 | (m) | small radius of positron | Chapters 3, 4, 6 |
| $2(R_c + r_p)$ | 7.8411E-13 | (m) | thickness of proton (neutron) | Chapters 6, 7, 8, 9 |

Notes:
(1) $R_c = 3.86159 \times 10^{-13}$  (m)   - is the Compton radius of
                            the electron.
(2) $1A = 10 \times 10^{-10}$  (m)      - is the Amstrong unit for length

# BSM-SG   Atlas of Atomic Nuclear Structures   Part II   Page: 0

## Shape symbols of nuclear atomic structures

n   p   D   T   He

## Sketch symbols of nuclear atomic structures

n   p   D   T   He

front view

bottom view

scale for nuclear structures and quantum orbits

← 1 Å →

Notations:

n - neutron
p - proton
D - deuteron
T - Tritii
He - Helium
Ar - Argon

EB - electronic bond (weak)
SGB - supergravitational bond (strong)
SGBclp - (proton) club proximity SGB
SGBpc - polar clamped SGB
PC - polar connection or clamp for Ar polar SGB

## Polar section vews

Argon nucleus (Ar)

Ar nucleus at the middle of nuclear chane of heavier atoms (Fig. 8.2 Chapter 8)

Ar nucleus at the end of nuclear chane of heavier atoms (Fig.8.2 Chapter 8)

## Simple quantum orbits (QOs)

(2)  (3)  (4)  (5)  (6)

(1)

(1) first harmonic QO (13.6 eV)
(2) second subharmonic QO (3.4 eV)
(3) third subharmonic QO (1.51 eV)
(4) fourth subharmonic QO (0.85 eV)
(5) fifth subharmonic QO (0.544 eV)
(6) sixth subharmonic QO (0.377 eV)

H2 - para state
(quantum orbits are in the perpendicular plane)

(1)

(1)

## Connection symbols

EB   SGBclp   SGBpc   PC

front view

bottom view

Example A   Example B

Example A: Two pairs of Ds connected by EB bonds
Example B: Two pairs of Ds conncted by SGBclp bonds

H2 -ortho (QO (1)  with 2 electrons with oposite spins)

(1)

Note: QOs for para and ortho states of H2 are normal to the proton's quasiplanes

# Periodic Table of atomic nuclear structures      (according to BSM-SG Unified Theory)
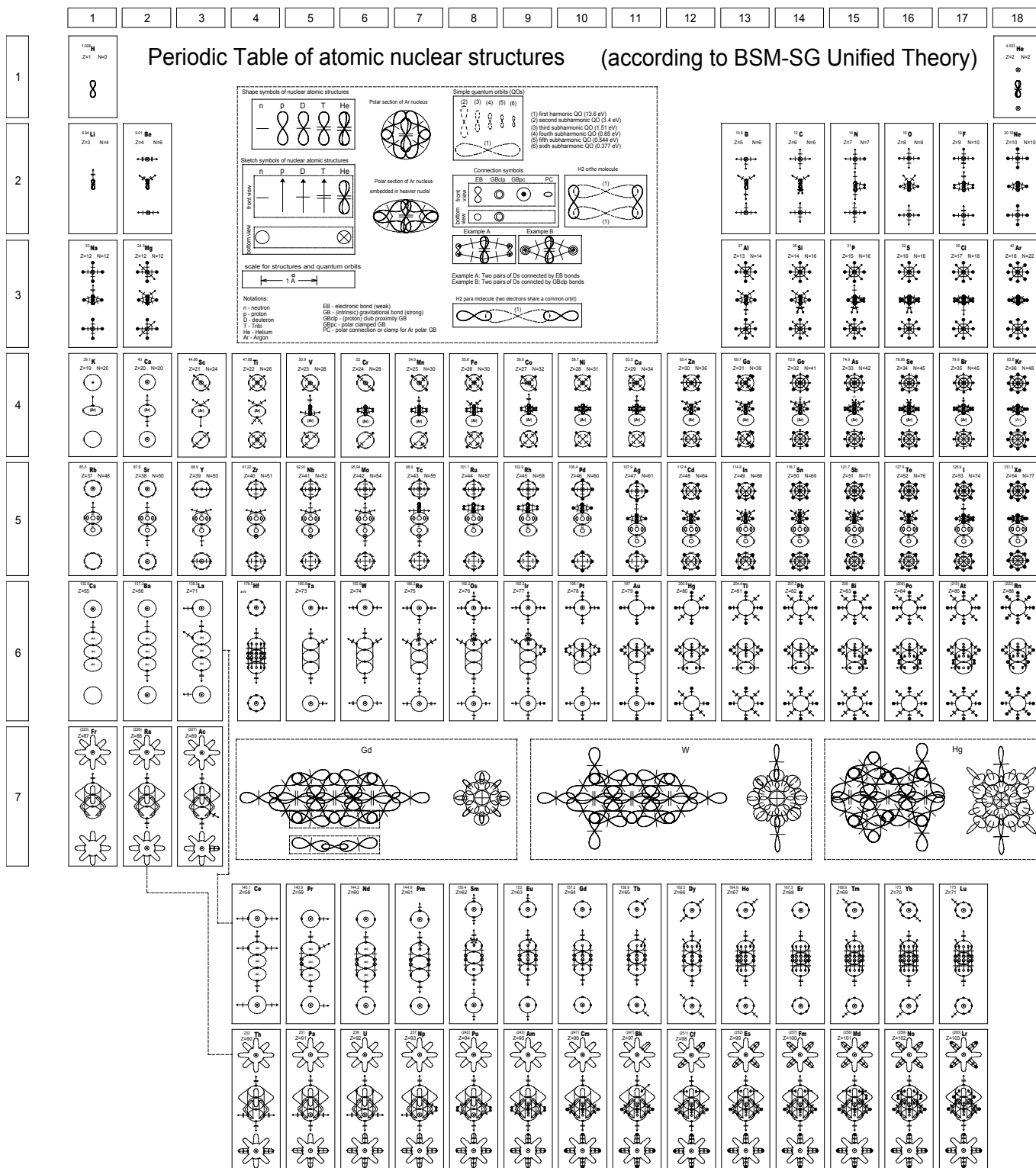
# Appendix: Derived equations and calculated physical parameters in BSM-SG

## 1. Derived equations:

**Notes**: 1. *The equation numbering is the same as in BSM chapters. The first digit corresponds to chapter's number.*

   2. *Equations (3.13.a), (3.21.a) and (3.42.F), known from the modern physics, are also derivable from the theoretical models of BSM.*

$$R_c = \frac{c}{2\pi\nu_c} \quad \text{Compton radius (BSM derivation)} \quad (3.13.a)$$

$$s_e = \frac{\alpha c}{\nu_c\sqrt{1-\alpha^2}} \qquad \text{Helical step} \qquad (3.13.b)$$

$$r_e = s_e/g_e \qquad \text{small electron radius} \qquad (3.13.c)$$

$$r_p = \frac{2}{3}r_e \qquad \text{small positron radius} \qquad (3.13)$$

$$c = \frac{\nu_R d_{nb}}{k_{hb}} \quad [\text{m/s}] \quad \text{light velocity by CL space} \quad (2.75)$$
$$\text{parameters}$$

$$\text{where:} \quad k_{hb} = \sqrt{1+4\pi^2(0.6164^2)} = 4 \quad (2.20.a)$$

$$\mu_o = \frac{4\pi m_{CL}k_{rd}^2 c\nu_c^3}{N_{RQ}} \quad \left[\frac{N}{A^2}\right] \qquad (2.52)$$

$$\varepsilon_o = \frac{N_{RQ}}{4\pi m_{CL}\nu_c^3 c^3 k_{rd}^2} \quad \left[\frac{C^2}{Nm^2}\right] \qquad (2.53)$$

$$h = \frac{\pi(c)c^2 m_{CL}N_{RQ}^3 k_d}{4\nu_c k_{hb}^3} \quad [\text{N m s}] \quad \text{where:} \quad k_d = \frac{\tau_{511KeV}}{\tau_{CL}} \quad (2.58)$$

$$q = \frac{N_{RQ}^2}{2\nu_c^2}\sqrt{\frac{c\alpha k_d}{2k_{rd}^2 k_{hb}^3}} \quad [\text{C}] \qquad (2.58.a)$$

$$P_S = \frac{g_e^2 h\nu_c^4(1-\alpha^2)}{\pi\alpha^2 c^3} \quad \left[\frac{N}{m^2}\right] \qquad (3.53)$$

$$\rho_e = \frac{m_e}{V_e} = \frac{g_e^2 h\nu_c^4(1-\alpha^2)}{\pi\alpha^2 c^5} \quad \left[\frac{kg}{m^3}\right] \qquad (3.55)$$

$$P_D = \frac{g_e h\nu_c^3\sqrt{1-\alpha^2}}{2\pi\alpha c^3} \quad \left[\frac{N}{m^2}\right] \qquad (3.62)$$

$$m = \frac{P_S}{c^2}V_H \quad [\text{kg}] \quad \text{- mass equation of FOHS} \qquad (3.48)$$

$$m = \frac{h\nu_c}{c^2}K_V \quad [\text{kg}] \quad \text{- mass equation of FOHS} \qquad (3.58)$$

$$\sigma = \frac{\nu_c\alpha^2}{2c} = 1.09737315\times10^7 \quad [(\text{m}^{-1})] \qquad (3.21.a)$$

$$\gamma = (1-V^2/c^2)^{-1/2} \qquad (3.42.F)$$

$$T = \frac{N_A^2}{S_w}\frac{h\nu_c(R_c+r_p)^3 L_{pc}^2}{2cR_c r_e R_{ig}}\left(\frac{\mu_e}{\mu_n}\right) \quad [\text{K}] \qquad (5.6)$$

$$T = \frac{N_A^2 hc^2\left(3g_e\sqrt{1-\alpha^2}+4\pi\alpha\right)^3}{864\alpha^3\nu_c^2\pi^2 g_e^2(1-\alpha^2)R_{ig}}\frac{\mu_e}{\mu_n} \quad [\text{K}] \qquad (5.12)$$

$$r^2 = b^2(1-a^2(\sin(\theta))^2) \qquad (6.54)$$

$$L_{pc} = \left[\left(\frac{\mu_e}{\mu_\mu}\right)^2(4\pi^2 R_c^2+s_e^2)-4n^2\pi^2 R_\pi^2\right]^{1/2} \qquad (6.61)$$

$$E = \frac{2q}{4\pi\varepsilon_0[L_q(1)+0.6455L_p]} = 16.01 \text{ eV} \text{ for } H_2 \text{ ortho} \quad (9.4)$$

$$C_{SG} = (2h\nu_c + h\nu_c\alpha^2)(L_q(1)+0.6455)L_p) \qquad (9.17)$$

$$\text{where:} \quad C_{SG} = G_0 m_{n0}^2$$

$$E_V = \frac{C_{SG}}{q[[[L_q(1)](1-\alpha^4\pi\Delta^2)]+0.6455L_p]^2} - \frac{2E_q}{q} - \frac{2E_K}{q} \quad (9.23)$$

$$\Delta r = L_q(1)\alpha^4\pi\Delta^2 \quad [\text{m}] \qquad (9.26)$$

$$\Delta E(p,n,\Delta) = \frac{2\alpha C_{SG}(A-p)^2}{[r_n\pm[\Delta r(n,\Delta)]]^2} - pB_{D2}(n,\Delta) \qquad (9.55)$$

$$P_P/P_S = \alpha^2/\sqrt{1-\alpha^2} \qquad (10.18)$$

$$p_p = \alpha c\rho_e = \frac{g_e^2 h\nu_c^4(1-\alpha^2)}{\pi\alpha c^4} = 2.19\times10^{-25} \quad \left[\frac{N \sec}{m^3}\right] \quad (10.22)$$

$$E_{IFM} = P_P V_e = h\nu_c\frac{v}{c}\alpha \qquad [Nm]\equiv[J] \qquad (10.11)$$

$$E_{IFM}^G = E_{IFM}\frac{\sqrt{U_{Gn}}}{2\alpha c} \qquad [J] \qquad (10.59)$$

$$r = \tilde{L}\frac{\ln(z+1)}{\ln(\tilde{n})} \qquad [\text{m}] \qquad (12.50)$$

$$\tilde{n} = \exp\left(\frac{1}{(dN/dz)(z+1)}\right) \qquad (12.52)$$

# 1. Table of derived equations        Table 1.

========================================

Eq. No   Parameter                    Name
--------------------------------------------------------------------------

(3.13.a)   $R_c$        Compton radius of electron
(3.13.b)   $s_e$        helical step of the electron
(3.13.c)   $r_e$        small electron's radius
(3.13)     $r_p$        small positron's radius
(2.75)     $c$        light velocity by resonance CL node param
(2.52)     $\mu_o$        permeability of free space
(2.53)     $\varepsilon_o$        permittivity of free space
(2.58)     $h$     Planck's constant by CL space parameters
(2.58.a)   $q$        unit charge by CL space parameters
(3.48)     m        (Newtonian) mass of FOHS expressed by
                       its volume $V_H$
(3.53)     $P_S$        Static CL pressure
(3.55)     $\rho_e$        Intrinsic electron density estimated by
                       the Newtonian mass
(3.58)     m     mass of FOHS expressed by volume ratio $K_V$
                       normalized to the electron envelope volume
(3.62)     $P_D$        Dynamical CL pressure
(3.57)     $m$     Newtonian mass of helical structure particle
(3.21.a)   $\sigma$     Rydberg constant by CL space parameters
(3.42.F)   $\gamma$     Relativistic gamma factor (derived from the
                       electron quantum motion
(5.6)      $T$     CL  background temperature (by e⁻ param)
(5.12)     $T$     CL  background temperature (by CL
                       space parameters)

*Note*: The calculated parameter $T$ is for the Earth local field

(6.54)                    Hippoped curve in polar coordinates
(6.61)     $L_{pc}$        Length of proton (neutron) core

(9.4)      E     Calculated energy potential for $H_2$ ortho-I,
                   corresponding to experimental value of EVIP
                   from PE spectrum

(9.17)     $C_{SG}$        Product of SG constant and the square of
                       intrinsic proton mass

(9.55)     $\Delta E(p, n, \Delta)$            Equation for vibrational
                   levels for diatomic homonuclear molecules,
                   where:  A - is the atomic mass in atomic mass
                   units (for one atom); p - is the number
                   of protons involved in the bonding system
                   (per one atom);
                   n - is a subharmonic quantum number of the
                   quantum orbit; $r_n$ - is the internuclear distance
                   at the equilibrium;  $\Delta r$ - is a deviation from
                   the equilibrium point;   $\Delta$ - is a vibrational
                   quantum number, referenced to equilibrium

(9.26)     $\Delta$ r        Range of vibrational motion of protons in
                       $H_2$ ortho-1 molecule

(10.11)   $E_{IFM}$        Inertial force moment of folded CL nodes

(10.18)   $P_P/P_S$        Ratio between Partial and Static CL
                       pressure

(10.22)   $p_p$        Specific partial pressure of CL space

(9.23)    $E_V$        Energy levels of $H_2$ ortho-I molecule

(10.59)   $E_{IFM}^G$        Inertial force moment in gravitational
                       field

(12.50)   r    cosmological distance between distant galaxies
                where: z - redshift; $\tilde{L}$ - mean intergalactic distance;

(12.52)   $\tilde{n}$        mean quasirefractive index of GSS;
            where:   $(dN/dz)$  -  is a  line density estimated from
                       Lyman alpha forests observations

# 2. Used physical constants        Table 2

========================================

Constant                            Name
-----------------------------------------------------------------

$\alpha = 7.29735308\times10^{-3}$                    fine structure constant

$c = 2.9979245\times10^{8}$     (m/s)     light velocity

$\nu_c = 1.2355898\times10^{20}$    (Hz)        Compton's frequency

$h = 6.6260755\times10^{-34}$     (J.s)        Planck's constant

$q = 1.60217733\times10^{-19}$    (C)        elementary charge

$\mu_0 = 4\pi\times10^{7}$            (N/A$^2$)     permeability of free space

$\varepsilon_0 = 8.8541878\times10^{-12}$  (C$^2$/N m$^2$) permittivity of free space

$g_e = 2.0023193$                electron's gyromagnetic factor

$\mu_e = 9.2847701\times10^{-24}$  (A m$^2$)  electron's magnetic moment

$\mu_n = 9.6623707\times10^{-27}$  (A m$^2$)  neutron's magnetic moment

**Notes:** (1) Additionally to the above constants, the rest masses of elementary particles as: proton, neutron, electron, pions, muon, kaon are used. Two parameters from Electroweak theory also are used - the Fermi coupling constants, $G_F$ and the effective mixing parameter $\theta_{eff}^{lept}$. The measured mass equivalent energies of the bosons and tau are also used.

(2) Large observational data material used by BSM is not presented in the abstract paper.

## 3. Calculated parameters　　　　Table 3

```
==================================================
Parameter                        Name
--------------------------------------------------
```

$R_c$ = 3.8615932×10$^{-13}$　(m)　Compton radius of electron

$s_e$ = 1.77061164×10$^{-14}$　(m)　helical step of the electron

$r_e$ = 8.842805×10$^{-15}$　(m)　small radius of the electron

$r_p$ = 5.895203×10$^{-15}$　(m)　small radius of the positron

$L_{pc}$ = 1.6277×10$^{-10}$　(m)　- proton's (neutron's) core length

$L_P$ = 0.667×10$^{-10}$　(m)　- proton's length

$W_P$ = 0.19253×10$^{-10}$　(m)　- proton's width

$2(R_c + r_p)$ = 7.841×10$^{-13}$　(m)　- proton's core thickness

$N_{RQ}$ = 0.88431155×10$^9$　number of resonance cycles contained in one SPM cycle

$\tau_{CL}$ = 0.0242631×10$^{-10}$　(s)　space-time constant of CL space

$k_d$ = 51.518　ratio between the CL pumping time for 511 KeV photon and the space-time const

$k_{hb}$ = $\sqrt{1 + 4\pi^2(0.6164^2)}$ = 4　- derived from the concept of wavetrain width and Airy disk in diffraction limited optics (Eq. 1.20.a)

$d_{nb}$ = 1.0975×10$^{-20}$　(m)　*xyz* node distance of CL space

$k_{rd}$ = 0.15　equivalent trace radius of vibrating MQ type of node normalized to a node distance

$m_{CL}$ = 6.94991×10$^{-66}$　(kg)　inertial mass of the CL node estimated from Eq. (2.58)

$T$ = 2.6758　(K)　CL space background temperature for the Earth local field

$P_S$ = 1.3735811×10$^{26}$　(N/m$^2$)　- Static CL pressure

$\rho_e$ = 1.52831×10$^9$　(kg/m$^3$)　- intrinsic electron density

$P_D$ = 2.0257865×10$^3$　(N/m$^2$Hz)　- Dynamical CL pressure

$E$ = 16.06　(eV)　- theoretically derived system energy, corresponding to $E_{VIP}$ = 15.967 eV from PE spectrum

$C_{SG}$ = 5.26511×10$^{-33}$　- (J m$^2$)　SG product

$\Delta r = 4 \times 10^{-16}$　(m)　- range of nuclear vibrational motion for $H_2$ ortho-I molecule

$p_p$ = 3.343482×10$^{15}$　(N sec/m$^3$) - specific partial CL pressure

```
==================================================
Parameter                        Name
--------------------------------------------------
```

$\nu_R$ = 1.092646 × 10$^{-29}$　(Hz)　CL node resonace frequency Eq. (2.55), (2.56)

## 4. Used abbreviations

| | |
|---|---|
| BSM-SG (BSM) | Basic Structures of Matter (theory) |
| CL | Cosmic Lattice |
| CL space | Cosmic Lattice space |
| EQ | Electrical Quasisphere |
| FOHS | First Order Helical Structure |
| FQHE | Fractional Quantum Hall Effect |
| SG | Super Gravitation |
| MQ | Magnetic Quasisphere |
| NRM | Node Resonance Momentum (vector) |
| RL | Rectangular Lattice |
| RL(R) | Rectangular Lattice (Radial) |
| RL(T) | Rectangular Lattice (Twisted) |
| SPM | Spatial Precession Momentum (vector) |
| SOHS | Second order helical structure |
| ZPE | Zero Point Energy |